The International Journal of Advanced Manufacturing Technology (2024) 133:5897–5925
https://doi.org/10.1007/s00170-024-14102-9

ORIGINAL ARTICLE

Development and characterization of hybrid aluminium matrix composites through stir-squeeze casting using distinct reinforcements for structural applications

Muhammad Asad Ali[1] · Nadeem Ahmad Mufti[1] · Kashif Ishfaq[1] · Rakhshanda Naveed[1] · Muhammad Qaiser Saleem[1] · Asif Mahmood Qureshi[2]

Received: 2 February 2024 / Accepted: 3 July 2024 / Published online: 10 July 2024
© The Author(s), under exclusive licence to Springer-Verlag London Ltd., part of Springer Nature 2024

Abstract

In the modern era, the demand for lightweight and high-strength aluminium matrix composites (AMCs) has significantly grown as a result of their structural applications in various sectors. The distinctive characteristics of AMCs are intricately impacted by variables like the type and weight percentage (wt.%) of reinforcement, the selection of processing techniques, and the matrix employed. Fabricating hybrid AMCs poses several challenges, including achieving desired geometrical shapes, homogeneous mixing of reinforcements, addressing porosity, and ensuring strong interfacial bonding of reinforcement-matrix interfaces. Stir-squeeze casting has emerged as a non-traditional casting technique with the potential to address these challenges effectively. This study intends to look into the impacts of the distinct reinforcement particles (Al_2O_3, SiC, Si_3N_4, and BN) with varying wt.% on the development of different configurations of hybrid AMCs based on AA2024. The key properties that have been examined include porosity, ultimate tensile strength (UTS), elongation percentage (EL%), hardness, and impact energy of developed hybrid AMCs. The results reveal that UTS (235.6 to 377.8 MPa) and hardness (51.5 to 85.1 HRB) significantly increased with the addition of reinforcement particles, while EL% (11.6 to 7.9%) and impact energy (6.62 to 5.61 J) decreased. AA2024/2%Al_2O_3/2%SiC/2%Si_3N_4/2%BN outperformed in terms of UTS and hardness and gave 60.36% and 65.24%, respectively; however, the porosity, EL%, and impact energy have been compromised from the matrix material (AA2024) by 1.61%, 31.89%, and 15.26%, respectively. Fractography analysis of UTS and Charpy impact fractured samples depicts that a dimple fracture has been observed for the AA2024 without any reinforcement. However, with the inclusion of particles for reinforcing (Al_2O_3, SiC), the fabricated AMC AA2024/2%Al_2O_3/2%SiC provided the cleavage fracture, while transgranular cleavage fractures have been observed in the fractured surfaces of the third and fourth configurations (AA2024/2%Al_2O_3/2%SiC/2%Si_3N_4, AA2024/2%Al_2O_3/2%SiC/2%BN). Moreover, the brittle fracture has been depicted in the broken sample of AA2024/2%Al_2O_3/2%SiC/2%Si_3N_4/2%BN.

Keywords Aluminium matrix composites · Stir-squeeze casting · Reinforcement particles · Ultimate tensile strength · Porosity · Impact energy

1 Introduction

Advances in the manufacturing industry have spurred a growing demand for enhanced strength, hardness, toughness, and impact resistance in advanced composite materials [1]. Composite materials are blends of two or more substances that cannot be separated and typically possess characteristics superior to those of the individual components [2]. The reinforcing and matrix materials of composite materials are the main factors that classify them. There are three types of matrix materials that can be distinguished: (i) metal matrix composites (MMCs), (ii) ceramic matrix

✉ Muhammad Asad Ali
asad.ali@uet.edu.pk

[1] Department of Industrial and Manufacturing Engineering, Faculty of Mechanical Engineering, University of Engineering and Technology, Lahore 54890, Pakistan

[2] Department of Mechanical Engineering, University of Engineering and Technology, Lahore 54890, Pakistan

composites (CMCs), and (iii) polymer matrix composites (PMCs). Composites can be categorized into three groups depending on the type of reinforcing material utilized: (i) particle-reinforced (micro and nanoparticles), (ii) fiber-reinforced (aligned and stapled), and (iii) structural (sandwich and laminate). MMCs have been identified as noteworthy developments in the manufacturing of advanced composites for various uses in the automotive, aerospace, and marine sector [3]. The widespread acceptance of MMCs is attributed to their superior toughness, strength, impact attributes, and high strength-to-weight ratio [4]. MMCs are made up of two main parts: (i) a matrix material, such as magnesium (Mg) or aluminium (Al), and (ii) reinforcing components, like fibers, whiskers, and particles [5]. When reinforcements are added, mechanical characteristics like toughness, hardness, and tensile strength are greatly improved over the underlying material [6]. However, in recent years, researchers' attention has shifted towards aluminium metal matrix composites (AMCs) due to their ability to alter physical, metallurgical, and mechanical characteristics through varying reinforcement particles and processing conditions [7]. Meeting the market demand for advanced composites can be achieved through the utilization of AMCs, given their cost-effectiveness and ease of production while maintaining desirable strength properties [8]. Since AMCs have advantageous characteristics like low weight, enhanced wear resistance, prominent strength, and minimal thermal expansion, AMCs are practiced in defense, automotive, and aerospace structural components [9–11].

Typically, the introduction of reinforcement particles to a low-strength matrix induces changes in its mechanical properties. Composites differ in their properties according to a number of criteria, including the kind, size, form, and wt.% of the reinforcing particles. AMC's can be created by incorporating and blending reinforcements like nitrides, oxides, borides, and carbides—examples include AIN, Si_3N_4, TiO_2, Al_2O_3, BN, TiB_2, B_4C, SiC, TiC, and Gr [12–14]. The processing methods and parametric conditions employed in the production of AMCs perform a crucial part in improving both the mechanical and microstructural attributes [15]. From a technological standpoint, solid-state and liquid-state processes are the two categories into which processing methods can be separated [16]. Liquid-state processing methods encompass techniques such as squeeze casting [17], ultrasonic-assisted casting [18], conventional stir casting [19], compo-casting [20], gravity die casting [21], centrifugal casting [22], and pressure-less infiltration [23]. On the other hand, solid-state processing methods involve plasma spark, microwave, and conventional sintering [24], as well as powder metallurgy (PM) [25]. The traditional fabrication methods for AMC development involved introducing and blending reinforced particles into molten aluminium through stir casting. However, these methods had drawbacks, including the potential for reinforcement segregation, hot tearing, center-line cracking, micro-porosities, and poor adhesion at the interface region between the metal matrix and reinforced particulates. These issues ultimately led to diminished mechanical and microstructural characteristics [26, 27]. Among the various casting processes, squeeze casting emerges as a non-traditional technique with the capability to address the aforementioned casting challenges. Squeeze casting offers advantages such as high strength, reduced cavities, minimal gas porosity, and the elimination of segregation caused by reinforcements, leading to an improved surface finish [28]. Additionally, it stands out as a highly efficient and effective method for producing near-net-shape products [29].

Mechanical and microstructural properties of AMCs developed through squeeze casting are highly influenced by reinforcement particle types, wt.%, and squeeze casting parametric conditions. Different researchers have worked on the development of AMCs and revealed improvements in their microstructural and mechanical characteristics. Singh et al. [30] undertook a study on AMCs reinforced with SiC, recognized as widely utilized engineering materials in aerospace and automotive applications. The authors investigated the formulation of a composite by introducing SiC into Al6063 at varying mass ratios (of 5%, 7.5%, 10%, 12.5%, and 15%) using the stir casting practice. Rendering to the findings, Al/SiC composites demonstrated a higher density compared to the pure aluminium matrix. The results also revealed a uniformly distributed particle structure, contributing to improved mechanical and microstructural attributes in the Al/SiC composites. Mourad et al. [31] employed squeeze stir casting to manufacture recycled AMCs, utilizing scrap aluminium alloy wheel (SAAW). Hybrid reinforcements, including alumina, SiC, and graphite, were incorporated to create environmentally sustainable AMCs. According to the results, adding 4% graphite and Al_2O_3 to SAAW improved strength while lowering frictional forces and wear rate. Microstructure exploration demonstrated that, in comparison to SiC, graphite and Al_2O_3 bonded to the SAAW matrix more successfully. In a different study, Christy et al. [32] concentrated on the processing, characteristics, microstructure, and optimization of SAAW reinforced with alumina, manufactured through squeeze and stir casting methods. A thorough investigation was performed on the stir-casted composites, taking into account the wear/tribological performance, microstructure, hardness, compression, and tensile strength. Both mechanical and tribological characteristics improved when alumina was added to the aluminium matrix.

Muraliraja et al. [33] used the squeeze casting method to develop an Al7075 AMC with a noticeably high compressive strength by adding 2.5% alumina as reinforcement. According to the authors, there was a 25.42% rise in AMC hardness. Furthermore, the composite's compressive strength

improved to 587 MPa with the inclusion of alumina reinforcement. Comparing this improvement to other recorded AMCs in the literature as well as the parent Al 7075 alloy was notable. The study research executed by Kumar et al. [34] aimed to examine the impacts of Al_2O_3/SiC reinforcing wt.% and size of particles on the mechanical and tribological characteristics of AA2024/Al_2O_3/SiC. The authors came to the conclusion that hybrid composites showed improved wear resistance and mechanical characteristics, which made them especially well-suited for uses like engine cylinder liners in the automotive sector. Lu et al. [35] conducted a thorough investigation of the distinct effects of Zr and Fe particle surplus on the microstructural attributes and mechanical behavior of Al7075/40%SiC. According to the findings, Zr particles had the best retention efficiency. On the other hand, when Fe particles are present, an average thickness of 12 µm hard, brittle Fe-Al layer appears on the surfaces of the Al matrix and Fe particles.

Bimetal composites produced by melt infiltration casting (MIC) and squeeze infiltration (SI) were examined on the bases of their microstructural, mechanical, and wear characteristics in a study by Gecu and Karaaslan [36]. Both processes were carried out at 625 °C. Under identical test conditions, the composite generated via SI showed somewhat better wear resistance. It underwent reduced abrasive wear and plastic deformation in comparison to the composite generated using MIC. SI seemed more beneficial while requiring a larger initial outlay of funds, particularly in light of its possible industrial application. Using the squeeze casting method, Venkata Rao et al. [37] synthesized the hybrid AMC, which is made of AA6061 reinforced with Al_2O_3/SiC. The following were found to be the ideal process parameters: a melt temperature (M_T) of 750 °C, a squeeze pressure (S_P) of 100 MPa, a pressure holding period (P_D) of 20 s, and the use of die steel material. In the hybrid AMC fabricated, this combination showed ideal values for yield strength, UTS, and hardness. Idrisi and Mourad [38] formulated the AMCs by employing two distinct methodologies: conventional and ultrasonic-assisted stir castings. Various concentrations of 40-µm-sized SiC microparticles (3%, 5%, 8%, and 10%) were utilized in the production of AMCs. Through microstructural examinations, the authors observed an even dispersion of SiC microparticles in the metal matrix by employing the ultrasonic method. Additionally, the findings showed that operating the ultrasonic-assisted stir casting method resulted in considerable improvements in both mechanical and physical characteristics. Chak and Chattopadhyay [39] evaluated the effectiveness of SiC-reinforced AMCs produced through the stir-squeeze casting. Microstructural examination revealed homogeneous SiC dispersion and refinement of grain in the aluminium. The authors concluded that the introduction of SiC reinforcement resulted in a notable enhancement of approximately 62% in UTS and 30% in microhardness compared to matrix.

From the literature cited above, it has been found that various reinforcement particulates have been utilized in the fabrication of AMCs. Single-type reinforcing materials, particularly those with low weight percentages, make it difficult for AMCs to combine physio-mechanical, microstructural, and thermal characteristics in a balanced way. Although increasing the reinforcement percentage enhances the strength properties of AMCs, it frequently results in decreased ductility and fracture toughness. Both ductility and fracture toughness are critical attributes for avoiding failures under in-service stress conditions. High percentages of reinforcement in composites can lead to issues such as high porosity and agglomeration. Therefore, replacing a single-reinforcement type with a specific weight percentage with two or more different reinforcements at their respective wt.% may help mitigate agglomeration problems. While numerous studies have focused on the fabrication of AMCs to enhance mechanical attributes compared to monolithic materials and other types of reinforced aluminium composites, it is noteworthy that limited research has explored the addition of more than two inorganic reinforcements in the AMCs of AA2024. For instance, Al_2O_3, SiC aluminium composites, and other single-reinforcement matrix composites have been developed to meet industrial requirements for mechanical attributes. Notably, substantial progress has been made in the development of hybrid composites, such as Al_2O_3/SiC-based composites, which are considered promising for high-strength applications. However, the combined effects of reinforcement oxides (Al_2O_3), carbides (SiC), and nitrides (Si_3N_4 and BN) have not been comprehensively explored, despite being preferred reinforcements in the industry. Furthermore, the influence of these reinforcements has not been significantly examined for the development of improved microstructural and mechanical characteristics of AMCs. Therefore, this study aims to develop hybrid AMCs based on different wt.% of hybrid reinforcement particles (Al_2O_3, SiC, Si_3N_4, and BN) through stir-squeeze casting. A thorough analysis has been performed to obtain how hybrid reinforcement particles affect the microstructural and mechanical characteristics of AMCs with regard to density and porosity (%), ultimate tensile strength (UTS), elongation percentage (EL%), hardness (HRB), and impact energy (IE). Microscopy and scanning electron microscopy (SEM) have been used to analyze the microstructure of hybrid AMCs. The key objectives of the current study are the following:

- Development of different configurations of hybrid AMCs through stir-squeeze casting.
- Microstructural and mechanical characterization of developed hybrid composites.

2 Materials and methods

This study's primary goal is to investigate the ways in which vital aspects of stir-squeeze casting affect both the microstructural and mechanical attributes of hybrid AMCs. This section presents a concise overview of the material selection and fabrication process/experimental procedures, as well as the characterization and mechanical testing employed in this study.

2.1 Materials selection

Compared to other series of aluminium alloys, the 2000 series has better embedding characteristics, such as increased damage tolerance and a stronger resistance to fatigue fracture propagation. This is why the aerospace, defense, maritime, and heavy transport vehicle-building industries use these alloys extensively [28, 40, 41]. Widely used in a variety of commercial applications, wrought aluminium alloy 2024 (AA2024) is utilized in wing tension members, ribs, fuselage structures, shear webs, and structural sections that call for exceptional strength, stiffness, and fatigue performance [42–45]. So, AA2024 has been chosen as the matrix for the fabrication of hybrid AMCs; the material's chemical composition is validated using optical emission spectroscopy and is displayed in Table 1.

In this study, hybrid AMCs were fabricated using various inorganic reinforcement particles such as Al_2O_3, SiC (with an average size of 35 nm), BN, and Si_3N_4 (with an average size of 100 nm). The reinforcement particles (Al_2O_3, SiC, BN, and Si_3N_4) have been selected on the bases of their specific properties and utilization in various applications as mentioned in Table 2, while the weight percentage (wt.%) has been selected on the bases of recommended range in literature [45–50]. The composition of different designed configurations of hybrid AMCs, along with their respective reinforcement types and weight percentages, is presented in Table 3. For each configuration, the wt.% of all reinforcement particles has been kept at 2%, while the overall wt.% of reinforcements has varied at 0%, 4%, 6%, 6%, and 8%, respectively.

2.2 Fabrication process

For the production of hybrid AMCs, a non-traditional casting method known as stir-squeeze casting was utilized. The specific process parameters are provided in Table 4. An electric resistance furnace with a heating capacity of 1000 °C

Table 1 Chemical composition of matrix material AA2024

Element	Cu	Ti	Si	Mn	Ni	Mg	Al
wt.%	3.87	0.03	0.19	0.63	0.02	1.25	Balanced

Table 2 Reinforcement particles selected for the development of hybrid AMCs

Reinforcements	Properties	Applications	References
Al_2O_3	➢ High strength-to-weight ratio	➢ Connecting rods ➢ Cylinder heads ➢ Pistons ➢ Brake discs	[45, 47]
SiC	➢ Thermal properties ➢ High hardness and stiffness ➢ High specific strength ➢ Resistant to acids, alkalis, and molten salts up to 800 °C	➢ Engine cradle ➢ Pistons ➢ Calipers ➢ Brake rotors ➢ Connecting rod ➢ Liners ➢ Propeller shaft ➢ Driveshaft ➢ Brake disc on ICE bogies	[48, 49]
BN	➢ Low density ➢ Lamellar crystalline structure with prominent lubricating attributes ➢ High thermal conductivity and low expansions ➢ High strength and hardness ➢ Superior shock resistance	➢ Automobile applications	[50]
Si_3N_4	➢ High tensile strength and hardness	➢ Automotive parts	[46]

Table 3 Composition of the designed configuration of hybrid AMCs under different reinforcements

Configurations		Matrix metal	Reinforcement particles			
		AA2024 (wt.%)	Al_2O_3 (wt.%)	SiC (wt.%)	Si_3N_4 (wt.%)	BN (wt.%)
A	AA2024	100	0	0	0	0
B	AA2024/2%Al_2O_3/2%SiC	96	2	2	0	0
C	AA2024/2%Al_2O_3/2%SiC/2%Si_3N_4	94	2	2	2	0
D	AA2024/2%Al_2O_3/2%SiC/2%BN	92	2	2	0	2
E	AA2024/2%Al_2O_3/2%SiC/2%Si_3N_4/2%BN	92	2	2	2	2

Table 4 Stir-squeeze casting parametric constant conditions to fabricate hybrid AMCs

Casting parameters	Description	Values
Melt temperature (M_T)	Controlled temperature of molten composite slurry that is transferred into the die cavity	800 °C
Reinforcement particle preheating temperature (R_T)	Temperature required to preheat the reinforcement particles to remove moisture contents and lubricants, to enhance the wettability with matrix metal	950 °C
Squeeze pressure (S_P)	Pressure applied to the plunger on the molten composite slurry for compression	100 MPa
Pressure duration (P_D)	The time interval during which the squeeze pressure is exerted on the molten material till the point of solidifying is reached	120 s
Die temperature (D_T)	The temperature at which the metallic die needs to be preheated prior to pouring the composite melt slurry	250 °C
Time delay (T_D)	The duration between the moment when the composite slurry is transmitted into the cavity and the subsequent initiation of the squeeze pressure on the slurry	15 s
Stirring speed (S_S)	The rotational speed of the stirrer necessary to accomplish a homogeneous mixture of the molten matrix material and the reinforced particulates	600 rpm
Stirring time (S_T)	The time duration in which molten slurry of composite is mixed during the stirring mechanism	5 min

was employed to melt the aluminium AA2024 matrix material while maintaining a superheat temperature of 800 °C. In order to improve the bonding between the molten metal matrix and the reinforcement particles, the designated wt.% of particulate reinforcements were preheated in a separate furnace at 950 °C for a duration of 3 h before the casting process. Once the AA2024 matrix reached the superheat temperature of 800 °C, slag was taken out of the melted slurry. Subsequently, the preheated reinforcement particles were introduced directly into the AA2024 melt. The melt was constantly stirred at 600 rpm for 5 min to make sure an even scattering of the particulate reinforcements throughout the melt. The action of stirring facilitates the dispersion of the reinforcing particles and improves the interfacial connection with the metal matrix.

In the meantime, the H13-forged steel die was subjected to preheating at a temperature of 250 °C using an oxyacetylene torch, in accordance with the suggestions put forth by prior research investigations. The temperature of the die was verified using an infrared temperature gun (Smart Sensor: AR330). Following the preparation of the composite slurry consisting of the mixture of AA2024 and reinforcement particles through stirring, it was cautiously added to the hot die cavity. The elapsed time between the application of squeeze pressure and the complete filling of the cavity with the molten composite slurry was meticulously measured and consistently maintained at approximately 15 s. To compress and solidify the molten composite slurry, a 100-ton vertical hydraulic press was employed. S_P of 100 MPa was applied to the composite slurry for 2 min to compress and solidify it. After releasing the squeeze pressure, the solidified billet of hybrid AMC was carefully extracted from the die. The resulting fabrication billet possessed dimensions of 140 mm × 56 mm × 54 mm. Figure 1a provided a general schematic illustrating the fabrication process of hybrid AMCs, while Fig. 1b highlighted the real-time process flow utilized for the development of hybrid AMCs through the stir-squeeze casting process. Various configurations (A, B, C, D, and E) of hybrid AMCs have been developed by varying distinct particulate reinforcement types and wt.%, as outlined in Table 3. The fabrication procedure was carefully followed to produce the different configurations through stir-squeeze casting based on the specific process parametric condition highlighted in Table 4, while three billets were fabricated for each configuration of hybrid AMCs.

Fig. 1 **a** Schematic illustration of the squeeze-casted hybrid composite process and **b** experimental flow process

2.3 Characterization and mechanical testing

2.3.1 Density and porosity (%)

Upon completing the fabrication of the hybrid AMCs, samples were prepared for density (g/cm^3) and porosity (%) testing by cutting them using a machining process specific to each configuration. The theoretical density of matrix metal AA2024 is 2.78 g/cm^3, while the theoretical densities of reinforcement particles Al_2O_3, SiC, BN, and Si_3N_4 are 3.95 g/cm^3, 3.21 g/cm^3, 2.1 g/cm^3, and 3.44 g/cm^3, respectively. However, the theoretical density of hybrid AMCs has been calculated according to the rule of mixing by using Eq. 1 [51].

$$\rho_t = (wt_{r1} \times \rho_{r1} + wt_{r2} \times \rho_{r2} + \ldots . + wt_{rn} \times \rho_{rn}) + wt_m \times \rho_m \quad (1)$$

where ρ_t represents the theoretical density of hybrid AMC; wt_{r1}, wt_{r2}, and wt_{rn} are the wt.% of reinforcement particles from 1 to n; and ρ_{r1}, ρ_{r2}, and ρ_{rn} are the respective theoretical densities of reinforcement particles from 1 to n, whereas wt_m and ρ_m are the wt.% and theoretical density of matrix material (AA2024). In accordance with the BN-75/4051–10 standard, the hydrostatic weighing approach (Archimedes principle) was used to determine the experimental density and porosity of various developed configurations of hybrid AMCs. After weighing each sample in both air and water, the actual or experimental density of each was calculated using Eq. 2 [52].

$$\rho_e = \frac{m_1}{m_1 - m_2} \times \rho_W \quad (2)$$

where ρ_e, m_1, m_2, and ρ_W indicated the experimental density, mass of hybrid AMC in the air and in the water, and the water density, respectively. The porosity of different hybrid AMCs has been measured using Eq. 3 [53].

$$Porosity(\%) = \frac{\rho_t - \rho_e}{\rho_t} \times 100 \quad (3)$$

2.3.2 Mechanical characteristics

The evaluation of the mechanical characteristics of the hybrid AMCs produced through stir-squeeze casting involved the assessment of various responses, including ultimate tensile strength (UTS), elongation percentage (EL%), hardness, and impact energy (IE). Shaper and milling machines have been employed to make the specimens for UTS, hardness, and IE testing. Tensile specimens were made in accordance with the ASTM-E8 standard, as depicted in Fig. 2a. A universal tensile testing machine (Model: UH300kNA) with a 30-ton capacity has been used for UTS testing at a strain rate of 5×10^{-3} mm/s and at ambient temperature. For each configuration of developed hybrid AMCs, three tensile samples have been tested, while their average value has been considered for the final analysis of UTS and EL%. EL% has been calculated by the following Eq. 4.

$$EL\% = \frac{L_f - L_i}{Li} \times 100 \quad (4)$$

where L_i and L_f are the initial and final gauge lengths of the tensile specimen, they have been measured by Vernier caliper as shown in Fig. 2a.

The amount of impact energy that the specimen absorbed during fracture was ascertained using the Charpy impact test. The preparation of the Charpy impact specimens adhered to the ASTM-E23-07a standard. These specimens were characterized by dimensions of 50 mm × 10 mm × 10 mm and featured a V-notch. The V-notch had a 45° angle, was 2 mm deep, and a 0.25 mm radius along the base side of one of the larger dimensions. The specimen's schematic illustration of the Charpy impact specimen has been provided in Fig. 2b. The impact energy absorbed by the specimen, resulting from the applied impact load, was quantified using the expression provided in Eq. 5.

$$IE_{absorbed} = mgR(cos\theta_2 - cos\theta_1) \quad (5)$$

where IE = impact energy, m = mass of fork, g = gravitational acceleration, R = the radius of the fork, θ_1 = initial reference angle or angle of fall, and θ_2 = final reference angle or angle at the end of the swing. For each configuration of fabricated hybrid AMCs, three Charpy impact specimens have been tested, and their average reading is taken as the final measurement of IE for the analysis.

The hardness of the developed hybrid AMCs has been assessed as per the ASTM E18-17 standard, utilizing a Rockwell hardness tester as depicted in Fig. 2c. The hardness testing was performed using the HRB scale, employing a steel ball indenter with a diameter of 1/16″. Ten seconds of dwell time were maintained, while a force load of 100 kgf was applied. Five distinct spots on the hybrid AMCs' surface were chosen for hardness measurements in each configuration to guarantee representative findings. After that, the mean value of the hardness measurements at these sites was determined and taken into account for further examination.

2.3.3 Microstructural characterization

Using common metallographic methods, the hybrid AMC specimens' microstructures were investigated. After the specimens were divided into smaller pieces, grit sizes of 60 and 100 of emery paper were used for a coarse grinding process. The goal of this coarse grinding stage was to

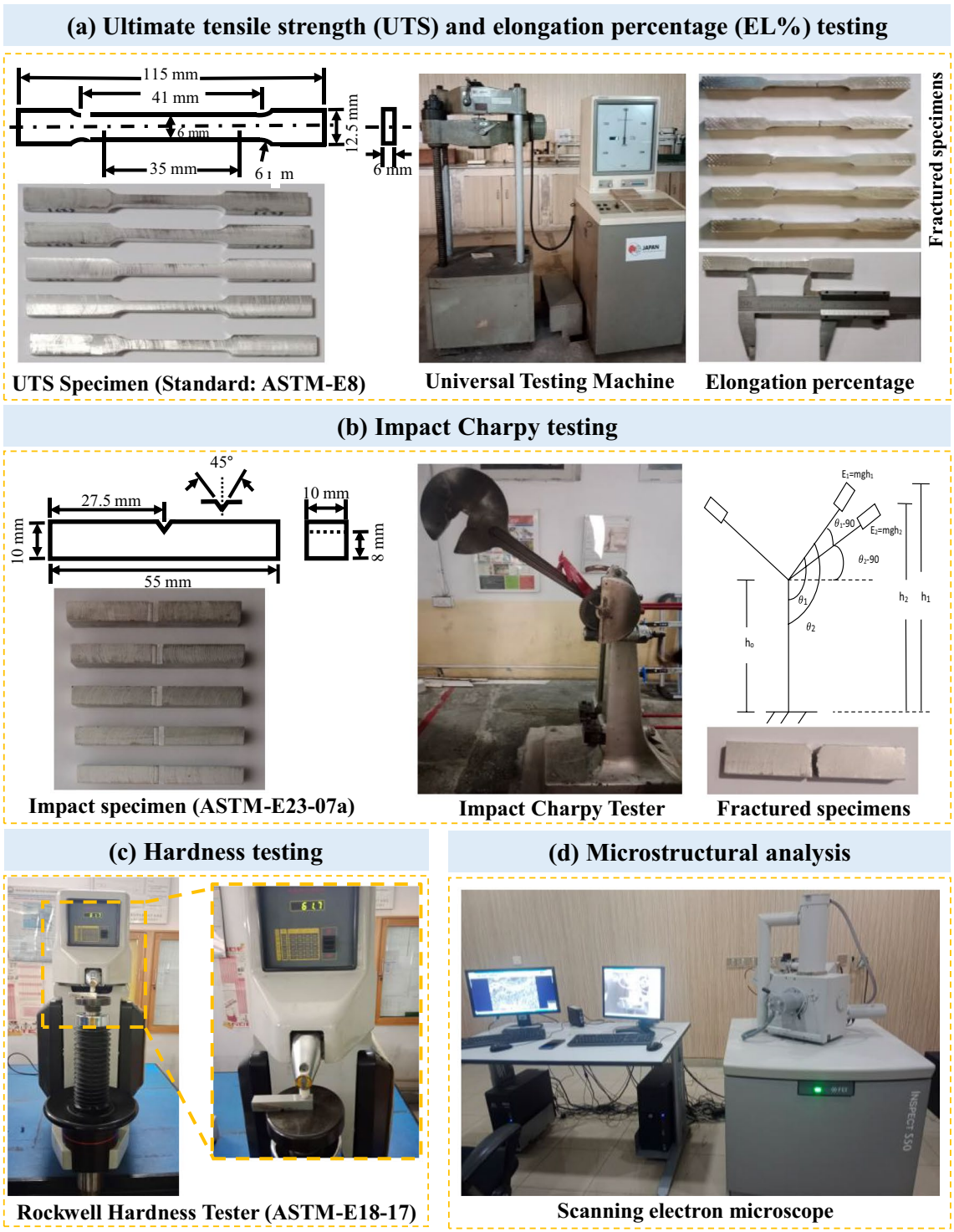

Fig. 2 Characterization and mechanical testing: **a** UTS and EL%, **b** impact Charpy testing, **c** hardness testing, and **d** microstructural testing

provide a smooth surface that would act as a base for further grinding operations. Following the coarse grinding phase, alcohol was used to thoroughly clean the samples. The next processes involved medium and fine grinding, using emery papers with grit levels ranging from 300 to 1000. The specimens were then polished with a velvet cloth coated in diamond paste to produce a surface that resembled a mirror. The polishing process involved rotating the cloth at a speed of 200 rpm in 5-min intervals. A Modern-1 Double Disc Grinder/Polisher was used to

complete the polishing process. After being ground and polished, the samples were etched using Keller's etchant, which included 190 mL of distilled water, 3 mL of HCl, 2 mL of HF, and 5 mL of HNO_3. The etching procedure took 20 s to complete. An optical microscope and a scanning electron microscope (FEI Inspect S50) were employed for microstructural analysis, as shown in Fig. 2d.

3 Results and discussion

In this research, the fabrication of hybrid AMCs of AA2024 has been carried out using different types of reinforcement particles with distinct wt.%. After the fabrication/development of hybrid AMCs, the hybrid AMCs are tested regarding their density and porosity (%), UTS (MPa), EL%, hardness (HRB), and impact energy (J). The results of this current study are in Table 5.

3.1 Density and porosity (%)

In this section, we meticulously examine the theoretical density (g/cm^3), experimental density (g/cm^3), and porosity (%) across various configurations of squeeze-cast hybrid AMCs, by varying wt.% of reinforcement particles: (A) AA2024, (B) AA2024/2%Al_2O_3/2%SiC, (C) AA2024/2%Al_2O_3/2%SiC/2%Si_3N_4, (D) AA2024/2%Al_2O_3/2%SiC/2%BN, and (E) AA2024/2%Al_2O_3/2%SiC/2%Si_3N_4/2%BN. Figure 3 encapsulates the outcomes pertaining to the theoretical density, experimental density, and porosity (%) of different hybrid AMC configurations. Utilizing Eqs. 1–3, we have calculated both theoretical and experimental densities, as well as porosity (%). It is noteworthy that the experimental densities, though marginally lower, closely align with the theoretical densities, underscoring the unavoidable presence of porosity in all samples. This porosity is inherent in the fabrication process of AMCs, stemming from procedural steps. The results reveal a direct correlation between density values and the escalation of reinforcement wt.%. Intriguingly, a non-linear relationship

Table 5 Results of UTS, EL%, hardness, and impact energy testing of developed hybrid AMC specimen

Configurations	UTS (MPa)	EL (%)	Hardness (HRB)	Impact energy (J)
A. AA2024	235.6	11.6	51.5	6.62
B. AA2024/2%Al_2O_3/2%SiC	284.8	9.7	65.7	5.78
C. AA2024/2%Al_2O_3/2%SiC/2%Si_3N_4	328.2	8.7	74.6	5.58
D. AA2024/2%Al_2O_3/2%SiC/2%BN	337.7	8.3	72.9	5.63
E. AA2024/2%Al_2O_3/2%SiC/2%Si_3N_4/2%BN	377.8	7.9	85.1	5.61

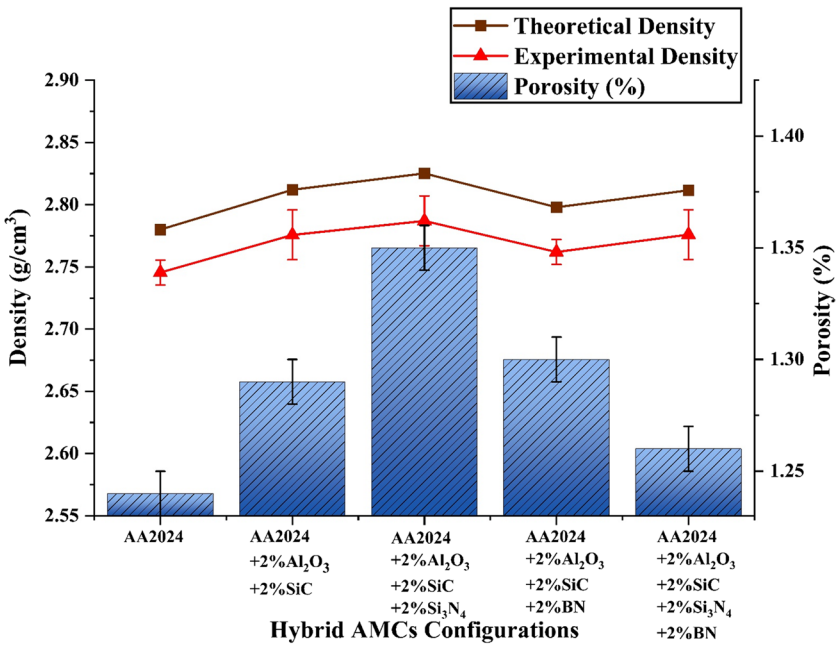

Fig. 3 Theoretical and experimental density with porosity (%) analysis of hybrid AMCs

is discerned with porosity as the wt.% increases. This non-linear trend sheds light on the intricate dynamics between reinforcement content and material density, offering insights into the nuanced behavior of these hybrid AMCs during fabrication. Figure 3 illustrates that squeeze-casted AA2024 exhibits the lowest porosity (1.24%) and, correspondingly, the lowest densities (ρ_t = 2.78 g/cm^3, ρ_e = 2.746 g/cm^3) when no reinforcement particles are incorporated into the AA2024 melt. This phenomenon arises from the absence of reinforcement particles that typically contribute to both porosity and density enhancement. The microscopic image presented in Fig. 4 further showcases the presence of minimal porosity and voids within the microstructure of squeeze-casted AA2024. Additionally, fine grain structure and dendrites are evident in the microstructure of squeeze-casted AA2024.

When introducing 2% Al_2O_3 and 2% SiC into the AA2024 melt, depicted in Fig. 3, both porosity (1.29%) and densities (ρ_t = 2.812 g/cm^3, ρ_e= 2.776 g/cm^3) of the squeeze-casted AMC (AA2024/2%Al_2O_3/2%SiC) exhibit an increase. This density augmentation in the hybrid AMC results from the higher densities of Al_2O_3 and SiC than AA2024, contributing to elevated theoretical and experimental densities. Concerning the porosity of the hybrid AMC (AA2024/2%Al_2O_3/2%SiC), the porosity of the hybrid AMC has grown with the involvement of reinforcements. This rise in porosity (%) is attributed to gas molecules entrapped during the stirring process, enriching the porosity during solidification. Numerous flaws, such as shrinkages, micropores, and microvoid cracks, are caused by this phenomenon. The microstructure of the hybrid AMC (AA2024/2%Al_2O_3/2%SiC) is revealed in Fig. 5, a microscopic image that shows the development of holes, voids, reinforcing particle presence, rosette-like structures, and small needle-like structures. The microstructure of hybrid AMCs includes rosette-like patterns, which are spiral or circular formations created by the interaction of the reinforcing particles (Al_2O_3 and SiC) with the molten metal (AA2024) during solidification. These structures take shape due to the AA2024 grains' preferred development around the Al_2O_3 and SiC reinforcing particles, which produces a unique pattern. Although the microstructure of AMCs often exhibits small, needle-like features, these structures are usually the result of the eutectic reaction that takes place during solidification between the reinforced particulates and the aluminium matrix (AA2024). As a result of this eutectic reaction, fine precipitates or needle-like phases form, which can have an influence on the mechanical attributes and microstructural characteristics of AA2024/2%Al_2O_3/2%SiC composite.

Regarding the hybrid AMC characterized by the addition of 2%Al_2O_3/2%SiC/2%Si_3N_4, as presented in Fig. 3, it exhibits the highest porosity (1.35%) and elevated densities (ρ_t = 2.825 g/cm^3, ρ_e = 2.787 g/cm^3). Figure 3 illustrates that the inclusion of 2%Al_2O_3/2%SiC/2%Si_3N_4 reinforcement particles significantly increases the density of the hybrid AMC (AA2024/2%Al_2O_3/2%SiC/2%Si_3N_4). This density augmentation can be recognized to the particularly higher density of Si_3N_4 (3.44 g/cm^3) compared to AA2024 (2.78 g/cm^3), leading to a substantial increase in both theoretical and experimental densities. Despite incorporating reinforcement particles into the melt, the experimental density is somewhat compromised due to inherent manufacturing imperfections associated with the casting process. The specimens

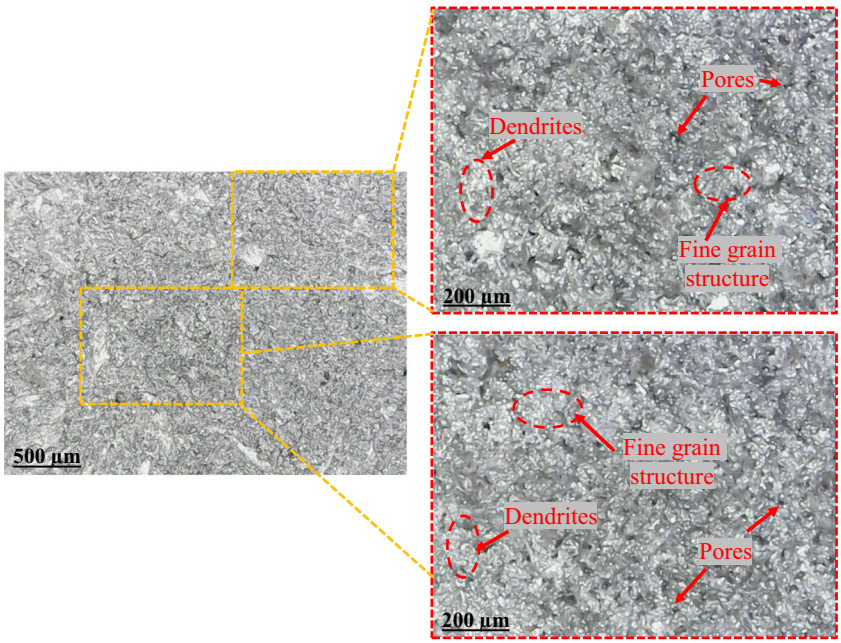

Fig. 4 Microstructural analysis of squeeze-casted AA2024

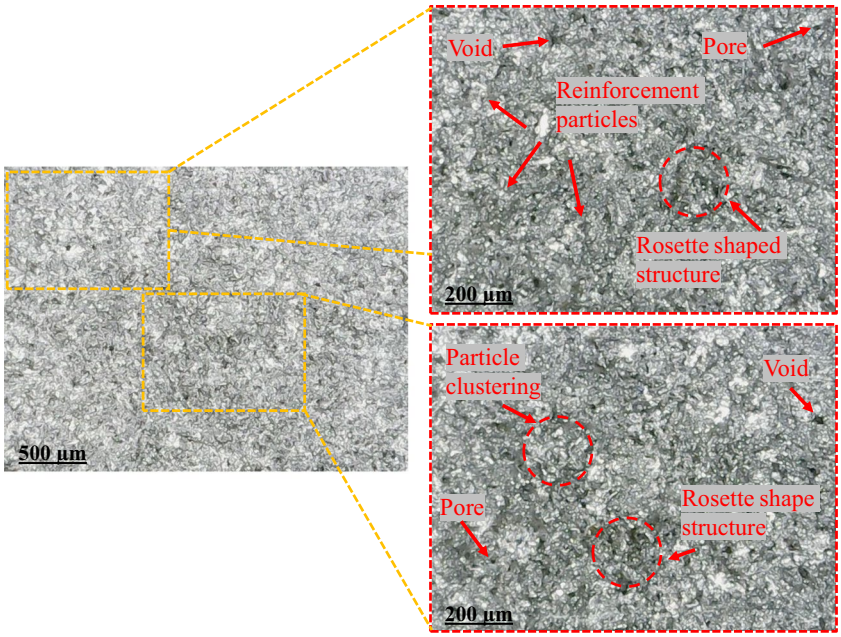

Fig. 5 Microstructural analysis of squeeze-casted AA2024/2%Al_2O_3/2%SiC hybrid composite

exhibit imperfections such as porosity, shrinkage, and slag inclusions, which can be traced back to the elevated temperatures employed in the molten metal formation process. Numerous variables contribute to the porosity observed in the composites. In the aluminium matrix (AA2024), the reinforcement particles are uniformly dispersed through agitation. This not only governs the accumulation of particles during the reinforcement content augmentation but also introduces gas into the molten metal as a byproduct of the stirring process. The entrapment of gas bubbles during solidification stands as the primary cause of porosity in the final structure. Consistent with prior research findings, the developed reinforced composites align well with expectations regarding their density and porosity [54]. The microscopic image shown in Fig. 6 indicated the greater porosity of blocky-shaped as well as the voids in the microstructure of squeeze-casted AA2024/2%Al_2O_3/2%SiC/2%Si_3N_4 hybrid AMC. Along with that, intermetallic compounds

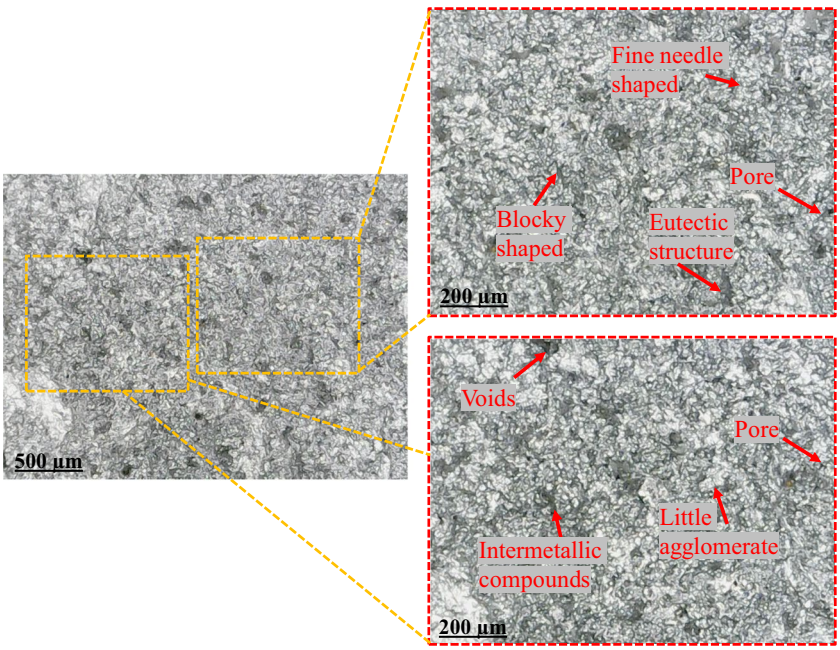

Fig. 6 Microstructural analysis of squeeze-casted AA2024/2%Al_2O_3/2%SiC/2%Si_3N_4 hybrid composite

and a little agglomeration are also observed on the squeeze-casted microstructure of hybrid composites.

The hybrid composite (AA2024/2%Al_2O_3/2%SiC/2%BN) exhibited some level of porosity (1.3%) and densities (ρ_t = 2.798 g/cm^3, ρ_e = 2.762 g/cm^3) with the incorporation of additional boron nitride (BN) reinforcement. In Fig. 3, it is highlighted that with the addition of BN, the porosity of the developed hybrid AMC has decreased. The reason is that BN has the lowest density (2.1 g/cm^3) compared to the other reinforcement particles as well as pure AA2024, which results in the depreciation of porosity. Another reason for the decrease in the porosity of hybrid AMC is that BN acts as the wetting agent, which reduced the porosity and did not produce any further cracks in the developed hybrid AMC. Several process parameters, including higher wt.%, stir time, and stir speed, contribute to the observed porosity in the composite. The duration of stirring in mechanical mixing offers a greater chance for atmospheric gases and oxides to become trapped, although it remains an essential parameter for ensuring proper mixing of particulates with the matrix during the molten state. While the wt.% of particles increases, turbulence and aggressive stirring can be created by maintaining a constant stir speed. This can lead to heterogeneous mixing and an increase in porosity. The microscopic image shown in Fig. 7 illustrated the eutectic structure of squeeze-casted hybrid AMC (AA2024/2%Al_2O_3/2%SiC/2%BN), where porosity and voids are highlighted on the microstructure.

When the wt.% of reinforcement particles such as 2%Al_2O_3/2%SiC/2%Si_3N_4/2%BN introduced in the melt of AA2024, then the porosity and density of the fabricated AA2024/2%Al_2O_3/2%SiC/2%Si_3N_4/2%BN depreciated due to the involvement of BN, which acts as the wettability agent and reduced the inhomogeneity of reinforcement particles, abridged the porosity (1.26%) and increased the densities (ρ_t = 2.812 g/cm^3, ρ_e = 2.776 g/cm^3) of the hybrid AMC, as depicted in Fig. 3. The microscopic image represented in Fig. 8 highlighted the small porosity and the voids in the microstructure of the hybrid AMC. The enrichment of intermetallic compounds and the fine needle-like structure have been seen on the microscopic image. The experimental study utilized optimal parameters to control additional porosity in the produced composites, preventing issues such as voids, local clustering, and agglomeration in the microstructure of hybrid AMCs. This meticulous control is essential for maintaining the mechanical characteristics of the composites, and the study found a lower porosity percentage due to the following considerations: (i) it is essential to use a vacuum atmosphere to protect the molten fluid from air contaminants when stirring; (ii) as a precautionary measure, the reinforcements are heated before melting and pouring; (iii) the molten matrix is combined with Al_2O_3/SiC/Si_3N_4/BN to ensure uniform wettability; and (iv) during the pouring operation and pressure application, a controlled delay period of 15 s is maintained to reduce the likelihood of air bubbles and gas blisters entering the atmosphere.

Figures 4, 5, 6, 7, and 8 demonstrated that the hybrid composite exhibits stronger interface bonding than the unreinforced AA2024 alloy. The load transmitted between the AA2024 and reinforcements is greatly affected by the

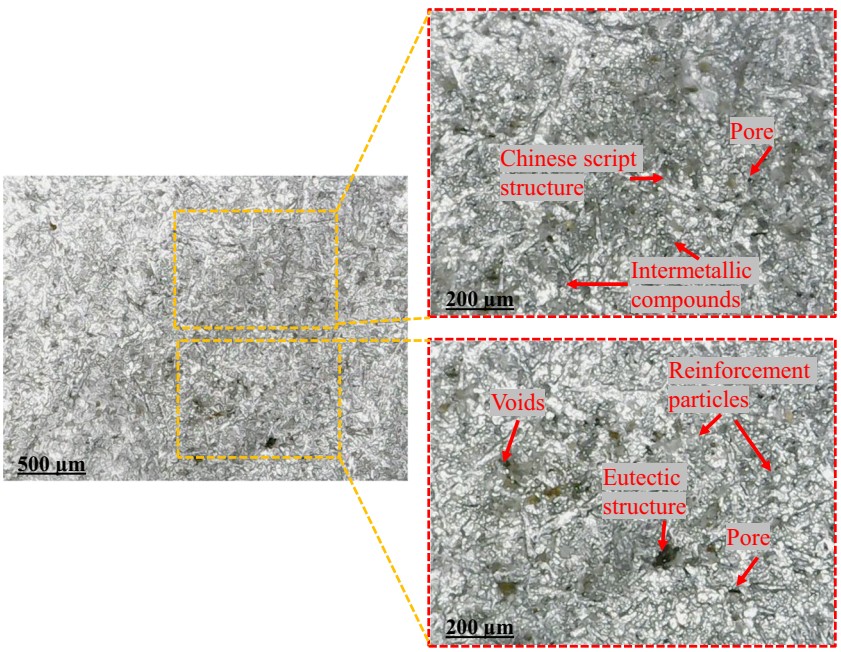

Fig. 7 Microstructural analysis of squeeze-casted AA2024/2%Al_2O_3/2%SiC/2%BN hybrid composite

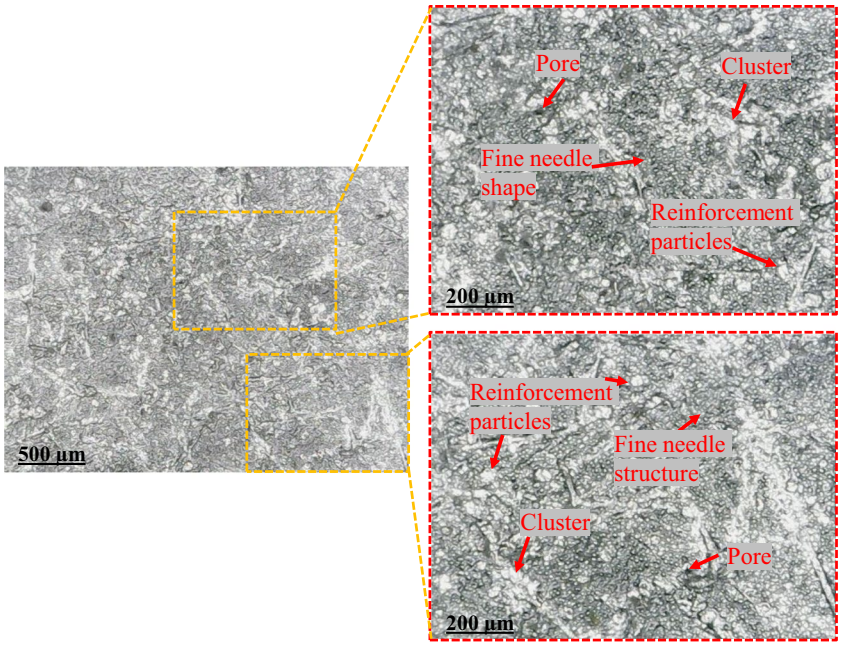

Fig. 8 Microstructural analysis of squeeze-casted AA2024/2% Al_2O_3/2%SiC/2%Si_3N_4/2%BN hybrid composite

strength of the interface bond. Interface binding strength is essential for the transmission of loads among them [55]. Because of their dislocation, the particles of Al_2O_3, SiC, Si_3N_4, and BN are dispersed, which inhibits mobility. It also contributes to the hybrid composite's increased mechanical strength. The microstructure further demonstrates the proper interfacial interaction between the AA2024 and the reinforcing particles. The reinforcements (Al_2O_3, SiC, Si_3N_4, and BN) are scattered all over the microstructure of the composites, with some particle clustering and strong interfacial bonding (Figs. 5, 6, 7, and 8). In all configurations of AMCs, no significant porosity is detected, and the range of porosity observed was between 1.24 and 1.35%. In certain cases, a moderate interfacial reaction may be necessary to create a strong and durable bond between the reinforcements and the metal matrix, leading to improved interfacial bonding.

3.2 Ultimate tensile strength

Figure 9 displays the results pertaining to the UTS (MPa) of various configurations of hybrid AMCs produced through squeeze casting, with respect to the wt.%: (A) AA2024,

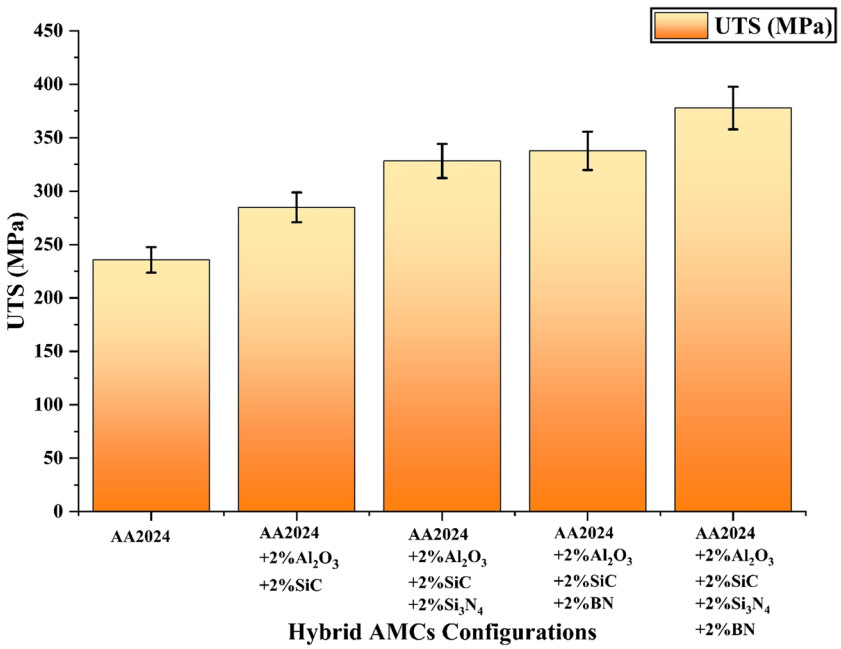

Fig. 9 UTS (MPa) analysis of hybrid AMC configurations

(B) AA2024/Al_2O_3/SiC, (C) AA2024/Al_2O_3/SiC/Si_3N_4, (D) AA2024/Al_2O_3/SiC/BN, and (E) AA2024/Al_2O_3/SiC/Si_3N_4/BN. Results reveal a direct correlation between the strength of hybrid AMCs and increased reinforcement wt.%. Figure 9 illustrates that squeeze-casted AA2024, with no reinforcement particles in the melt, exhibits the lowest UTS (235.6 MPa). The squeeze-casted AA2024 exhibited the lowest UTS compared to the other hybrid AMCs. The primary reason for the lowest UTS is linked to the absence of reinforcements, which prevents the enhancement of strength. The fractured sample is further examined with SEM analysis for the study of the porosity, cracks, and fracture structure. Hence, the SEM analysis presented in Fig. 10 provided additional evidence of porosity and crack propagation in fractured samples of squeeze-casted AA2024, concurrently revealing the presence of a dimple fracture structure. Ductile fractures typically exhibit surface features characterized by numerous small, round, or elongated depressions called dimples. These dimples arise as a result of localized stretching and tearing of the material during plastic deformation that occurs prior to the final fracture.

Upon the introduction of 2% Al_2O_3 and 2% SiC into the melt of AA2024, as depicted in Fig. 9, the UTS of the squeeze-casted AMC (AA2024/2%Al_2O_3/2%SiC) experienced an increase of 284.8 MPA, which is 20.88% improved than matrix material AA2024. The increased concentration of SiC and Al_2O_3 in the hybrid AMC as opposed to the base matrix AA2024 is responsible for its strength increase. The rise in dislocation density close to the reinforcement-matrix interface and the grain consolidation effect is caused by hard Al_2O_3/SiC reinforcement that is firmly bound to the AA2024 matrix [56]. The rise in weight percentage of hard and brittle SiC and Al_2O_3 particles, which impede dislocation motion, is the primary cause of the dislocation density increase. UTS of the hybrid AMCs was identified to be substantially greater when compared to the AA2024 metal matrix [57]. As the tensile loading is applied to the hybrid AMC, stress concentrations are generated, which causes the initiation and propagation of cracks. Due to this effect, reinforcement particles hinder crack propagation, and therefore, a higher load or force is required for the breakage of hybrid AMCs. Despite the existence of reinforcements in the hybrid AMC (AA2024/2%Al_2O_3/2%SiC), porosity, cracks, and their propagation are highlighted in the SEM analysis of the fractured sample, as shown in Fig. 11. The SEM analysis also indicates the separated grain boundaries of α-Al and the formation of cleavage-shaped structure on the fractured surface of hybrid AMC (AA2024/2%Al_2O_3/2%SiC). The evident separation of grain boundaries in α-Al reveals that the aluminium matrix (AA2024) of the hybrid AMC (AA2024/2%Al_2O_3/2%SiC) underwent grain boundary separation during the fracture process. This separation can be attributed to the applied stress surpassing the strength of the grain boundaries, leading to their separation and the creation of distinct boundaries between adjacent grains. Furthermore, the presence of a cleavage-shaped structure on the fractured surface implies that the fracture occurred along well-defined crystallographic planes within the material. Such a cleavage

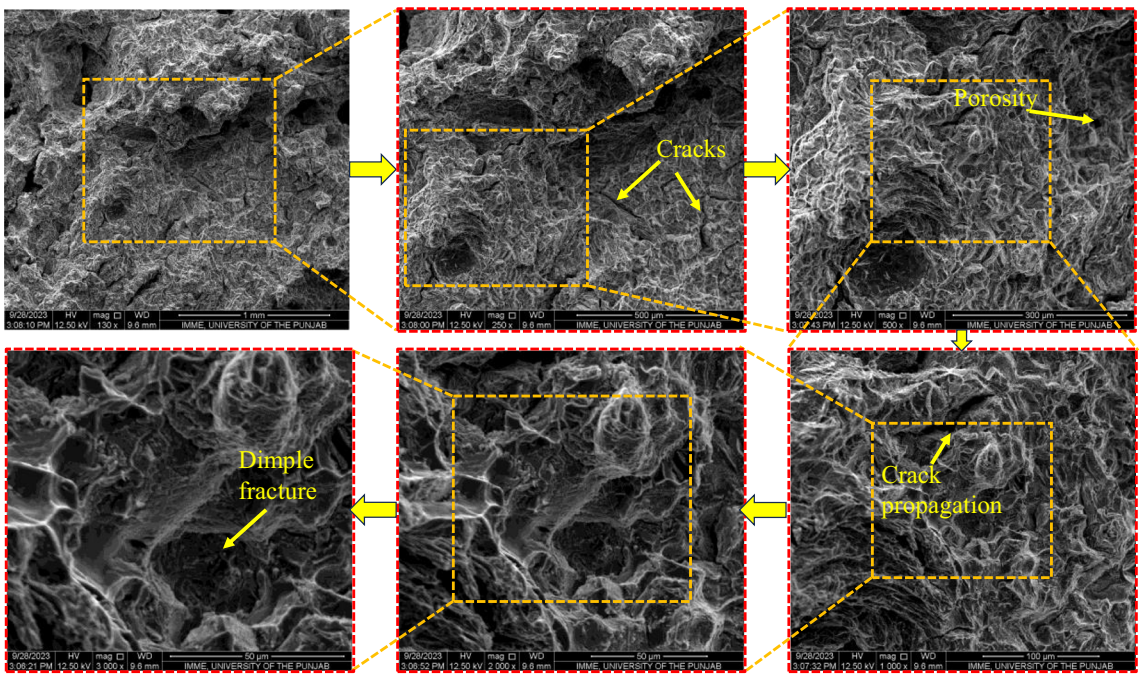

Fig. 10 SEM analysis of squeeze-casted AA2024 UTS specimen

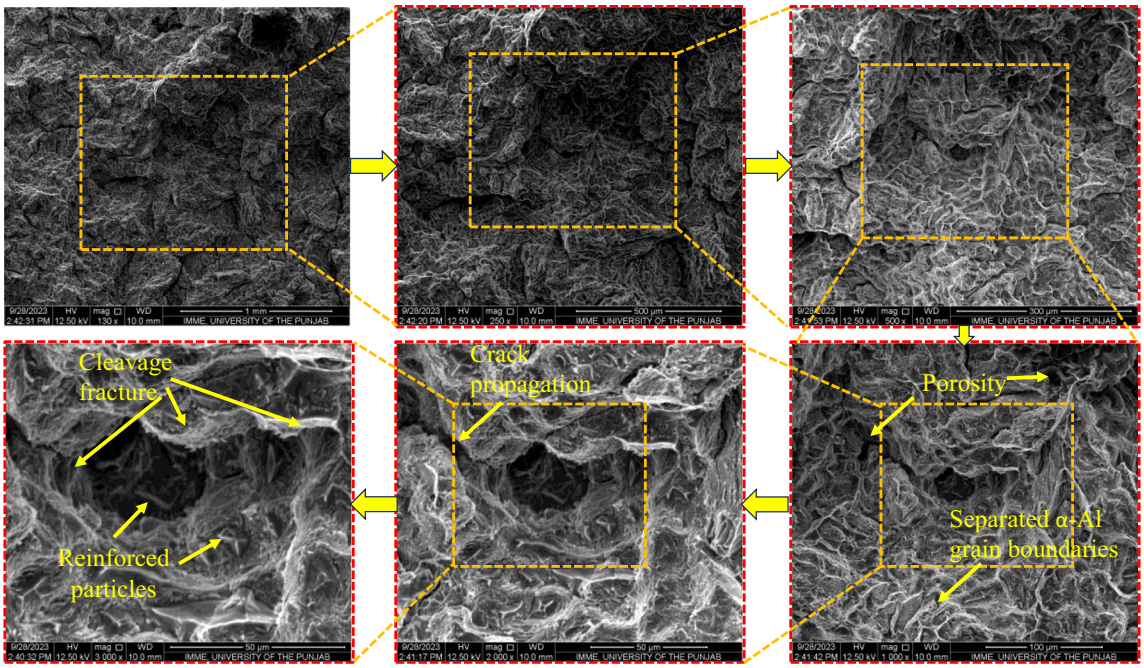

Fig. 11 SEM analysis of the fractured surface of squeeze-casted AA2024/2%Al_2O_3/2%SiC hybrid composite UTS specimen

fracture pattern, commonly observed in brittle materials, indicates that the fracture propagation followed specific crystal planes, resulting in a flat and smooth fracture surface characterized by distinct cleavage planes.

Examining the hybrid AMC incorporating 2% Al_2O_3, 2% SiC, and 2% Si_3N_4 in Fig. 9, it is evident that this composition yields a higher tensile strength (328.2 MPa) compared to the AA2024 (39.30%) and to AA2024/2%Al_2O_3/2%SiC (15.24%). The addition of 2%Al_2O_3/2%SiC/2%Si_3N_4 reinforcement particles significantly enhances the density of the hybrid AMC, contributing to increased tensile strength. Previous research suggested several ways to improve composites, including load sharing, particle strengthening, grain refining, and thermal mismatch strengthening enforced by reinforcement particles [58]. The ceramic particles help transfer the applied load more effectively from the aluminium matrix to the hard particles, which can bear a significant portion of the load, enhancing the overall tensile strength [59]. The presence of 2% Al_2O_3, 2% SiC, and 2% Si_3N_4 can lead to finer grain structures in the AA2024 (matrix material), which typically results in higher strength due to the Hall–Petch relationship [60]. Reinforcements like Si_3N_4 can help in deflecting and bridging cracks, thereby improving toughness and tensile strength. The crack has to navigate around or through these hard particles, which consumes more energy and delays failure [61]. Generally, increased porosity in composites can lead to reduced mechanical properties, including tensile strength, as pores act as stress concentrators and crack initiation sites. Despite the negative effect of porosity, the combination and distribution of the reinforcements (2%Al_2O_3/2%SiC/2%Si_3N_4) can still result in a net improve in tensile strength. This is due to the reinforcements' ability to significantly enhance the load-bearing capability of the AMC. If the distribution of porosity is not uniform and is primarily located in less critical areas, its detrimental effects might be less pronounced compared to the overall strengthening provided by the reinforcements. This could potentially contribute to the increased tensile strength of squeeze-casted hybrid AMC (AA2024/2%Al_2O_3/2%SiC/2%Si_3N_4). The transgranular cleavage fracture of the hybrid AMC is highlighted by the SEM examination of the fractured sample displayed in Fig. 12. Furthermore, on the fractured surface of hybrid AMC (AA2024/2%Al_2O_3/2%SiC/2%Si_3N_4), where distinct α-Al grain boundaries have been detected, porosity, cracks, and their propagation have also been observed. Rather than being along grain boundaries or other surfaces, the transgranular cleavage fracture suggests that the fracture happened through the material's interior. This type of fracture is typically associated with brittle materials and suggests that the hybrid AMC may have limited ductility and a tendency to fracture along well-defined crystallographic planes. The propagation of cracks indicates that the material experienced fracture propagation under applied stress. This indicates that the cracks initiated and grew, possibly due to stress concentration points or other factors, leading to the ultimate failure of the material.

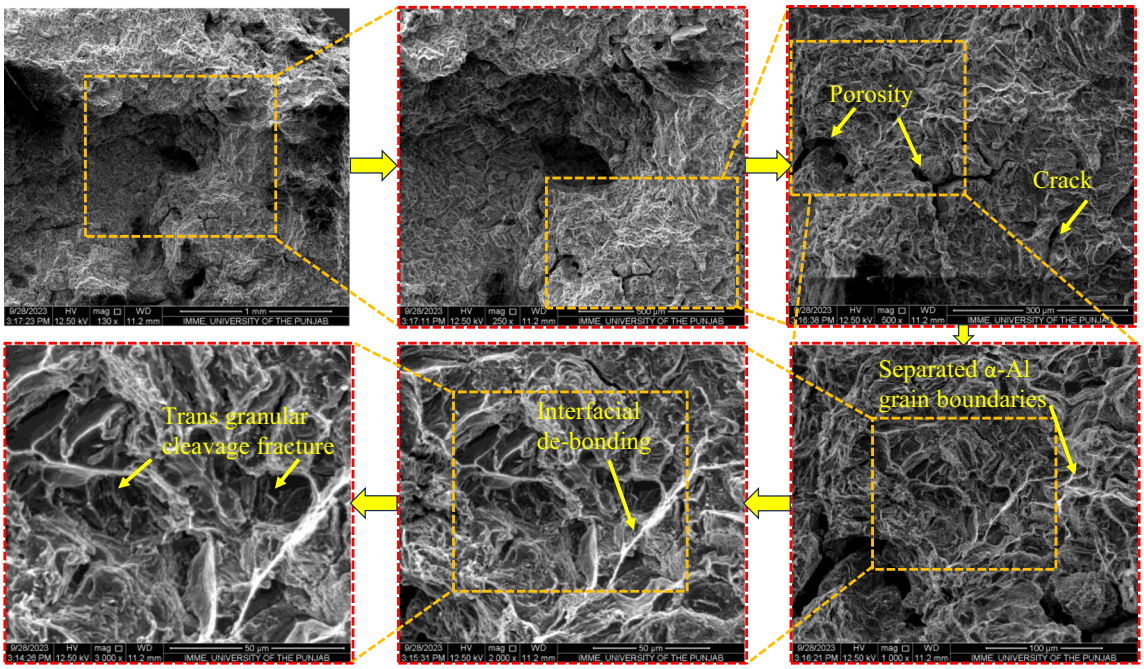

Fig. 12 SEM analysis of squeeze-casted AA2024/2%Al_2O_3/2%SiC/2%Si_3N_4 hybrid composite UTS specimen

The hybrid composite (AA2024/2%Al_2O_3/2%SiC/2%BN) displayed a degree of higher tensile strength (337.7 MPa), and this value of tensile strength is 43.34% improved than the AA2024, 18.57% improved than the AA2024/2%Al_2O_3/2%SiC, and 2.81% improved than the AA2024/2%Al_2O_3/2%SiC/2%Si_3N_4, and this tensile strength (337.7 MPa) has increased due to the introduction of additional BN reinforcements. In Fig. 9, it is observed that the incorporation of BN led to a reduction in the porosity and an increment in the UTS of the developed hybrid AMC. This enrichment in UTS can be recognized to the circumstance that BN contributes to the porosity reduction in the hybrid AMC through its role as a wetting agent, minimizing porosity, favoring the enhancement of UTS, and preventing the occurrence of further cracks in the developed hybrid AMC. This is because the crystalline structure of boron nitride has a lamellar structure and important lubricating characteristics. Furthermore, these materials have good shock resistance, minimal thermal expansion, high thermal conductivity, and outstanding workability [50]. Mechanical mixing over an extended stirring time provides more opportunities for the entrapment of atmospheric gases and oxides, although it remains crucial for ensuring proper mixing of particulates with the matrix during the molten state. The SEM analysis shown in Fig. 13 indicated the interfacial debonding of the fractured specimen of hybrid AMC (AA2024/2%Al_2O_3/2% SiC/2%BN), with the separated grain boundaries of α-Al. However, porosity, crack propagation, and transgranular cleavage fractures have been observed in the fractured SEM analysis of hybrid AMC (AA2024/2%Al_2O_3/2%SiC/2%BN). The broken specimen's interfacial debonding indicates that the interfaces between the aluminium matrix (α-Al) and the reinforcements (Al_2O_3, SiC, and BN) may have detached or separated. This reveals that during the fracture event, the applied stress was too great for the strength of the connection that holds the matrix (AA2024) and reinforcing particles together.

As illustrated in Fig. 9, the strength of composites generally tends to increase as the wt.% of reinforcements in the matrix material raises. The effective transmission of stress from the matrix to the reinforcements, the differences in the alloy and composite matrix failure behaviors, the introduction of a high density of dislocations into the matrix, and the shrinking of the composite grain size are some of the causes of this phenomenon. The deviation in the thermal expansion coefficients of the matrix alloy and the reinforcement could be the cause of this disparity [46]. The anticipation was that the abundant smaller particles 2%Al_2O_3/2%SiC/2%Si_3N_4/2%BN would enhance strength, as these small particles can effectively pin dislocations due to their strong strengthening capability. Furthermore, the ultimate tensile strength of hybrid AMC (AA2024/2%Al_2O_3/2%SiC/2%Si_3N_4/2%BN) demonstrates an increase of 60.36% when compared to AA2024, 32.65% when compared to AA2024/2%Al_2O_3/2%SiC, 15.11% when compared to AA2024/2%Al_2O_3/2%SiC/2%Si_3N_4, and 11.87% when compared to AA2024/2%Al_2O_3/2%SiC/2%BN. The fractographic investigation of the mechanical behavior indicates

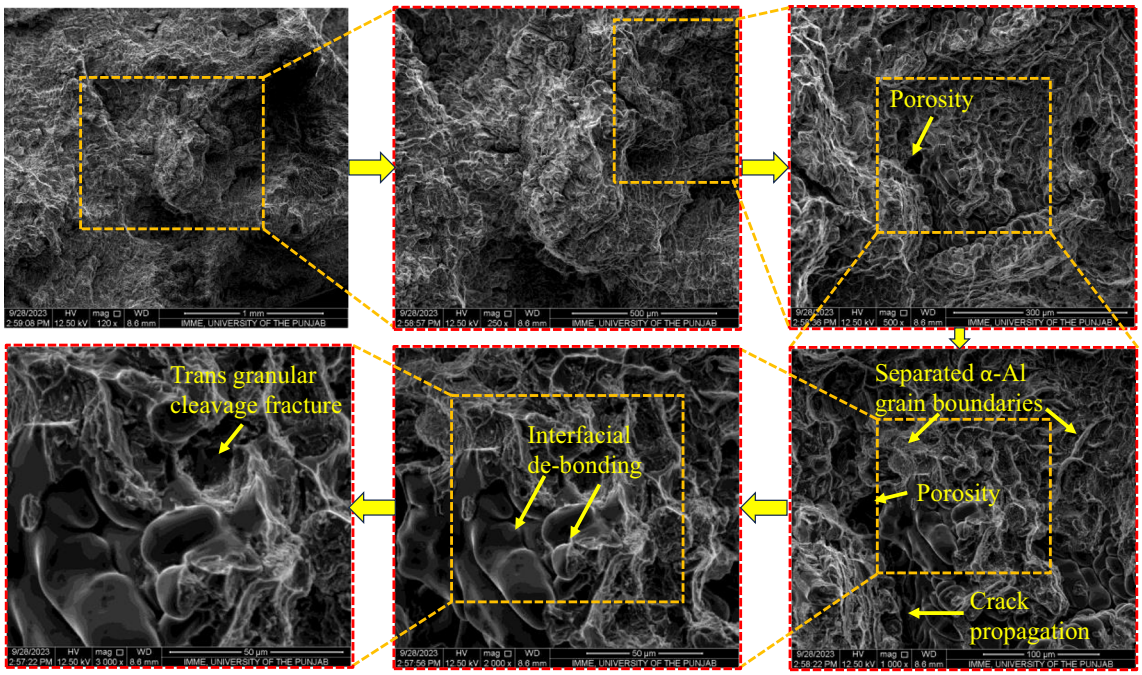

Fig. 13 SEM analysis of squeeze-casted AA2024/2%Al_2O_3/2%SiC/2%BN hybrid composite UTS specimen

that the AA2024 matrix alloy has a high degree of internal ductility, which allows it to efficiently distribute localized internal stresses. This internal ductility contributes to the overall mechanical resilience of the alloy. However, the presence of 2%Al_2O_3/2%SiC/2%Si_3N_4/2%BN particles limits the plastic flow of the hybrid AMC, leading to a fracture with a at higher tensile load or force. The SEM analysis shown in Fig. 14 revealed the interfacial debonding of the fractured specimen of hybrid AMC (AA2024/2%Al_2O_3/2%SiC/2%Si_3N_4/2%BN), with the separated grain boundaries of α-Al.

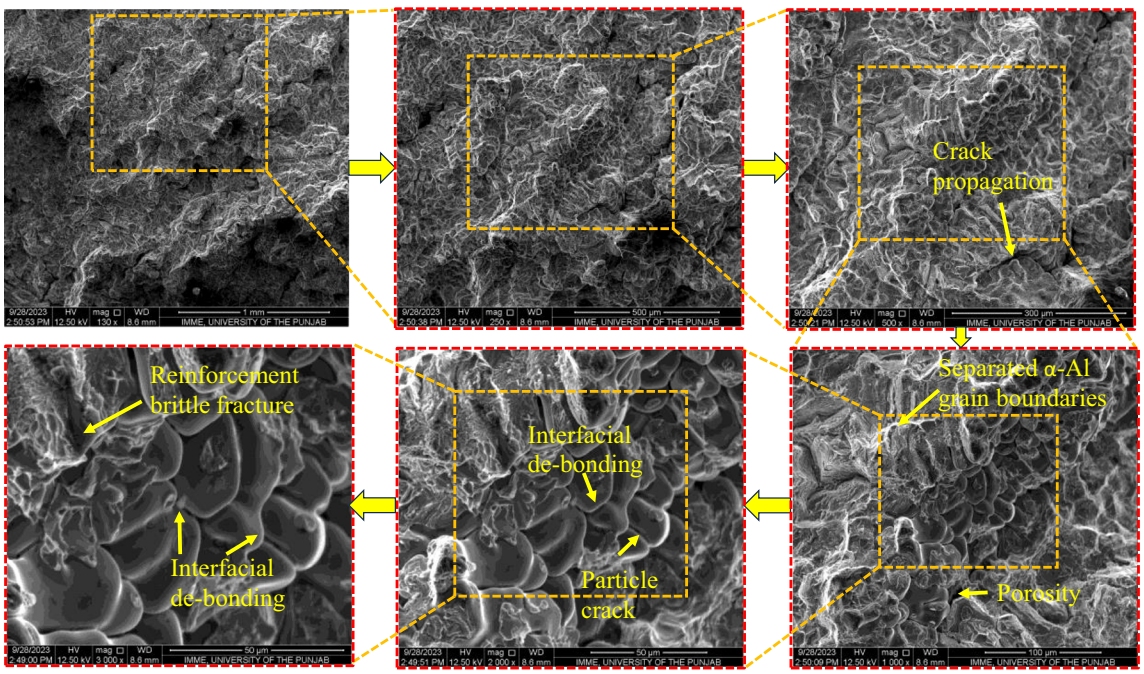

Fig. 14 SEM analysis of squeeze-casted AA2024/2%Al_2O_3/2%SiC/2%Si_3N_4/2%BN hybrid composite UTS specimen

However, porosity, crack propagation, and transgranular cleavage fractures have been observed in the fractured SEM analysis of hybrid AMC (AA2024/2%Al_2O_3/2%SiC/2%Si_3N_4/2%BN).

The SiC, Al_2O_3, Si_3N_4, and BN particles in the AA2024 matrix are what cause the increase in UTS and loss in ductility as wt.% of reinforcement increases. As the AA2024 matrix and the previously described reinforcements solidify, these reinforcements smooth out the grains and create a solid interfacial connection among them. When the tensile load is also transmitted from the matrix to the reinforcements in the AA2024/2%Al_2O_3/2%SiC/2%Si3N_4/2%BN hybrid composite due to its superior interfacial bonding resistance to dislocation motion compared to the AA2024, the reinforcement particles' supporting properties help the hybrid composite, which adds to its enhanced strength. The even dispersion of Al_2O_3, SiC, Si_3N_4, and BN particles is responsible for the increased UTS that results from the insertion of reinforcement.

3.3 Elongation %

Figure 15 presented the EL% results for various configurations of hybrid AMCs produced through squeeze casting, denoted as (A) AA2024, (B) AA2024/Al_2O_3/SiC, (C) AA2024/Al_2O_3/SiC/Si_3N_4, (D) AA2024/Al_2O_3/SiC/BN, and (E) AA2024/Al_2O_3/SiC/Si_3N_4/BN, corresponding to different wt.% of reinforcements. The outcomes exhibit an inverse correlation between the EL% of hybrid AMCs and the increased reinforcement wt.%. Specifically, Fig. 15 highlighted that squeeze-casted AA2024, lacking any reinforcement particles in the melt, displays the highest EL% (11.6%). The reason is that, without the reinforcement particle, bonding developed between the atoms is not of greater extent and gives a high strain rate when a specific load or force is applied. In comparison to the other hybrid AMCs, squeeze-casted AA2024 demonstrates the highest EL% (ductility), primarily attributed to the absence of reinforcement particles hindering strength enhancement.

When 2% Al_2O_3 and 2% SiC were introduced into the melt of AA2024, as illustrated in Fig. 15, the EL% (9.7%) of the squeeze-casted AMC (AA2024/2%Al_2O_3/2%SiC) exhibited a notable decrease, representing a 16.38% reduction over the base matrix material AA2024. The reason is that EL% exhibits a decline as the wt.% of reinforcement particles raises in AA2024. The incorporation of the reinforcements imposes constraints on the ductile characteristics of the alloy matrix (AA2024), attributed to the introduction of dislocations. Moreover, the robust bonding of hard and brittle Al_2O_3/SiC reinforcement to the AA2024 matrix contributes to increased dislocation density near the matrix reinforcement interface and a grain-strengthening effect. The heightened dislocation density is primarily a result of the increased wt.% of reinforcement particles, which hinders the dislocation motion and results in a decrease in EL% [62].

Analysis of the hybrid AMC incorporating 2% Al_2O_3, 2% SiC, and 2% Si_3N_4 in Fig. 15 revealed a significantly lower EL% (8.7%) compared to AA2024 (11.6%) and AA2024/2%Al_2O_3/2%SiC (9.7%). The addition of 2% wt.% each of Al_2O_3/SiC/Si_3N_4 reinforcement particulates contributes to a notable increase in the grain refinement during the solidification, making strong and hard interfacial bonding with the matrix material (AA2024), resulting in depreciation of ductility. Through the application of squeeze casting to

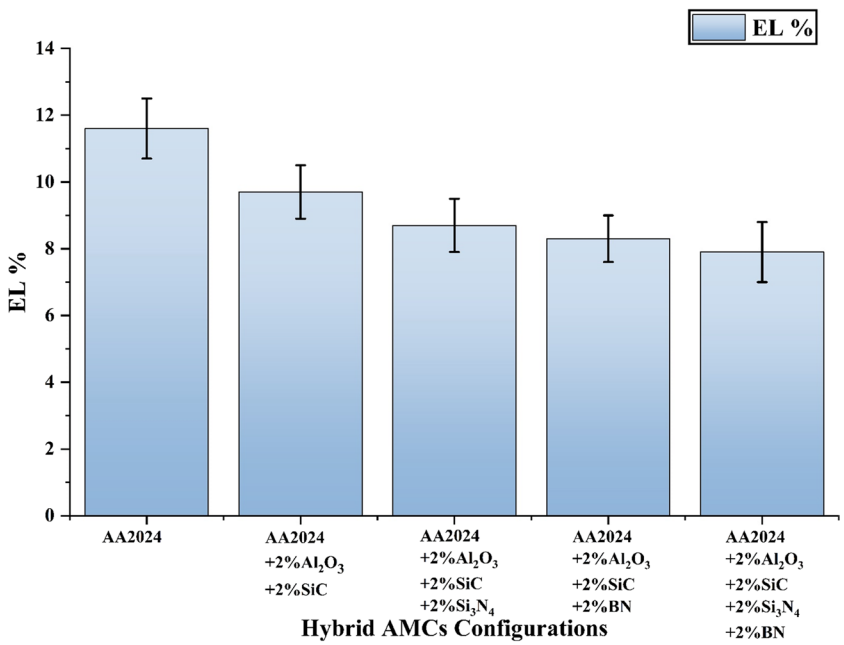

Fig. 15 EL (%) analysis of hybrid AMC configurations

these reinforcement particles, further grain refinement and a reduction in porosity were achieved, potentially contributing to the increased strength of the squeeze-casted hybrid AMC (AA2024/2%Al_2O_3/2%SiC/2%Si_3N_4). Additionally, the homogeneous stirring of reinforcement particles during fabrication reduced porosity, further enhancing the tensile strength of the hybrid AMC and resulting in a reduced EL%.

The hybrid AMC (AA2024/2%Al_2O_3/2%SiC/2%BN) demonstrated a notably lower EL% (8.3%), representing a 28.45% reduction over AA2024, an 14.43% reduction over AA2024/2%Al_2O_3/2%SiC, and a 4.59% reduction over AA2024/2%Al_2O_3/2%SiC/2%Si_3N_4 (Fig. 15). This reduced EL% (8.3%) is attributed to the introduction of additional BN reinforcements after the 4% addition of Al_2O_3 and SiC, making an overall 6% of reinforcement particles in the AA2024. In Fig. 15, it is evident that the incorporation of BN led to a reduction in porosity and a depreciation in the EL% of the developed hybrid AMC. This reduction in EL% can be linked to BN's role as a wetting agent, reducing porosity, promoting EL% reduction, and preventing the occurrence of further cracks in the developed hybrid AMC. However, homogeneous mechanical mixing offers fewer opportunities for the entrapment of atmospheric gases and oxides and, hence, produces a firm connection between the AA2024 and the reinforcement particles, resulting in a better EL%. Particles within the matrix may agglomerate or cluster as a result of the presence of reinforcement particles. Cracks may begin and spread earlier as a result of this clustering, which may serve as stress concentrators. The material's capacity to elongate before breaking is thereby diminished, making it more prone to failure under tensile pressure.

The EL% of AMCs (AA2024/2%Al_2O_3/2%SiC/2%Si_3N_4/2%BN) tends to reduce with a higher content of reinforcements within the matrix material, as illustrated in Fig. 15. Moreover, the EL% (7.9%) of the hybrid AMC (AA2024/2%Al_2O_3/2%SiC/2%Si_3N_4/2%BN) demonstrates a 31.89% decrease compared to AA2024, an 18.56% decrease compared to AA2024/2%Al_2O_3/2%SiC, a 9.19% decrease compared to AA2024/2%/Al_2O_3/2%SiC/2%Si_3N_4, and a 4.82% decrease compared to AA2024/2%Al_2O_3/2%SiC/2%BN. This phenomenon can be accredited to the effective transmission of stress from the matrix to the reinforcements by inducing high dislocation density in the hybrid AMC (AA2024/2%/Al_2O_3/2%SiC/2%Si_3N_4/2%BN) and hard interfacial bonding. The smallest EL% was because a substantial amount of reinforcement particles of Al_2O_3, SiC, Si_3N_4, and BN would enhance strength, given their capability to effectively pin dislocations due to their robust strengthening characteristics.

The insertion of reinforcement particles (Al_2O_3, SiC, Si_3N_4, and BN) can lower the EL% in squeeze-casted hybrid AMCs. The main cause of this is the reinforcing particles' intrinsic characteristics and how they interact with the matrix material (AA2024) during deformation. The previously stated reinforcing particles, which block the dislocations that are the primary carriers of plastic deformation in metals, fortify the AA2024. These particles induce the creation of barriers that hinder the dislocation motion and make the material's plastic deformation more difficult. This reduces the EL% by making the material stiffer and less ductile. The restrictions of the reinforcing particles on the material's ability to withstand strain and undergo plastic deformation result in a reduction of the material's total ductility. Moreover, the distribution and direction of the reinforcing particles inside the matrix may also have an influence on the mechanical aspects of the hybrid AMCs. If the particles are not aligned correctly or are not spread equally, the EL% could be further reduced. This could cause stress concentrations and promote the emergence and spread of cracks.

3.4 Hardness

This section provides a thorough analysis of the impact of various configurations of reinforcing particles on the hardness of squeeze-casted hybrid AMC. Hardness (HRB) was calculated by applying a Rockwell hardness tester according to the ASTM-E18-17 standard. Figure 16 presents the results related to the hardness (HRB) of various configurations of squeeze-casted hybrid AMCs based on wt.%: (A) AA2024, (B) AA2024/2%Al_2O_3/2%SiC, (C) AA2024/2%Al_2O_3/2%SiC/2%Si_3N_4, (D) AA2024/2%Al_2O_3/2%SiC/2%BN, and (E) AA2024/2%Al_2O_3/2%SiC/2%Si_3N_4/2%BN. The results depict a direct relation between the hardness values and the increase in reinforcement wt.% as shown in Fig. 16. Figure 16 revealed that squeeze-casted AA2024, without any reinforcement particles in the melt, exhibits the lowest hardness (51.5 HRB). The reason is that aluminium without the addition of reinforcement is comparatively a soft material and did not develop a strong bond within the atoms, therefore exhibiting a lower hardness.

When 2% Al_2O_3 and 2% SiC are introduced into the melt of AA2024, as depicted in Fig. 16, the hardness (65.7 HRB) of squeeze-casted hybrid AMC, i.e., AA2024/2%Al_2O_3/2%SiC, significantly increased by 27.57%. A suitable squeeze pressure and duration lead to heightened matrix density, constraining dislocation movement, and enhancing hardness [63]. In addition, the inclusion of rigid and durable alumina particles within the matrix acts as a barrier to plastic deformation during indentation. Because of this, the material's hardness is improved and its capacity to face plastic deformation is limited [64]. However, the presence of pores facilitates the easy movement of dislocations during indentation, causing the hybrid AMC (AA2024/2%Al_2O_3/2%SiC) to exhibit characteristics like a ductile material. Furthermore, the adoption of a S_p of

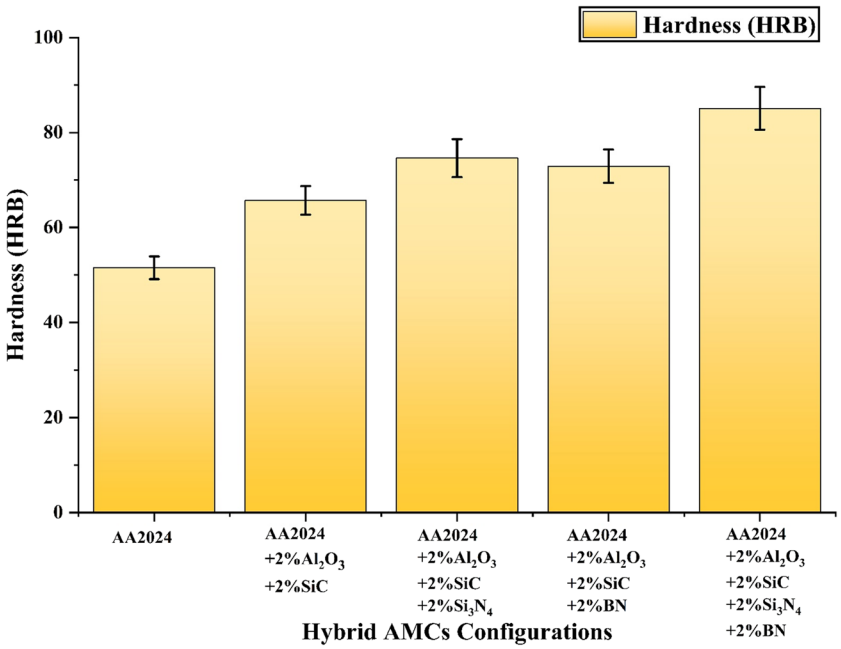

Fig. 16 Hardness (HRB) analysis of hybrid AMC configurations

100 MPa and a P_D of 2 min resulted in reduced porosity and consequently higher hardness in this study. The rise in hardness for the hybrid AMC is attributed to the higher hardness of AA2024/2%Al_2O_3/2%SiC compared to the base AA2024, causing the hardness to rise.

Regarding the significant enhancement in hardness (74.6 HRB) observed in the hybrid AMC, which is achieved through the addition of 2%Al_2O_3/2%SiC/2%Si_3N_4, the addition of Si_3N_4 reinforcement particles results in a notable improvement in hardness, as seen in Fig. 16, with its higher hard characteristics compared to AA2024, is a key contributor to this notable increase in hardness. Additionally, it was noted that the AA2024/Al_2O_3/SiC/Si_3N_4 hybrid composites' resistance to dislocation motion is that they have a higher hardness than the AA2024 alloy, and the intermetallic connection that exists between the reinforcement and matrix is strengthened by the addition of reinforcement.

The hybrid composite AA2024/2%Al_2O_3/2%SiC/2%BN displayed a certain degree of depreciation (2.28%) in hardness compared to the hybrid AMC based on 2%Al_2O_3/2%SiC/2%Si_3N_4 as shown in Fig. 16. This is due to the fact that the BN reinforcement particle has the lowest density, which results in a fall in hardness due to the improper bonding of the atoms of the hybrid AMC (AA2024/2%Al_2O_3/2%SiC/2%BN). In Fig. 16, it is emphasized that the addition of BN resulted in a reduction of porosity in the developed hybrid AMC. This reduction in hardness is attributed to BN having the lowest density (2.1 g/cm^3) compared to other reinforcement particles and AA2024, contributing to the mitigation of porosity.

Upon introducing a wt.% of reinforcement particles, specifically 2%Al_2O_3/2%SiC/2%Si_3N_4/2%BN, into the melt of AA2024, a notable increase in hardness (85.1 HRB) has been observed in the fabricated hybrid AMC (AA2024/2%Al_2O_3/2%SiC/2%Si_3N_4/2%BN), as shown in Fig. 16. Moreover, the hardness (85.1 HRB) of the hybrid AMC (AA2024/2%Al_2O_3/2%SiC/2%Si_3N_4/2%BN) demonstrates a 65.24% increase compared to AA2024, a 29.53% increment compared to AA2024/2%Al_2O_3/2%SiC, a 14.08% increase compared to AA2024/2%/Al_2O_3/2%SiC/2%Si_3N_4, and a 16.74% increase compared to AA2024/2%Al_2O_3/2%SiC/2%BN. Incorporating SiC and Si_3N_4 particles into the AA2024 has a notable impact on enhancing the composite's hardness. This outcome is anticipated because aluminium, being inherently soft, benefits from the introduction of hard SiC and Si_3N_4 particles, contributing positively to the overall hardness of the composite. The existence of SiC and Si_3N_4 reinforcement, known for their stiffness and strength, increases the resistance to plastic deformation during hardness testing. However, the effectiveness of this constraint relies on the uniform distribution of SiC and Si_3N_4 particles within the matrix. Uneven particle distribution, with clustering in certain areas and absence in others, can result in significant variations in hardness values across different locations in the specimen. Achieving a more uniform particle distribution is contingent upon dynamics such as stirring speed and time. Therefore, a blend of four different reinforcements (AA2024/2%Al_2O_3/2%SiC/2%Si_3N_4/2%BN) gave rise to high hardness with homogeneous stirring compared to other configurations used in this study.

When hard reinforcement particles (Al_2O_3, SiC, Si_3N_4, and BN) are added to the AA2024, they increase the hardness and transfer its characteristics from a ductile material to a brittle material. An increment in the wt.% of

reinforcements causes the matrix to become less wettable and less homogeneous, which raises the viscosity and makes it more difficult to pour the composite material. A few important variables influencing the hardness of hybrid AMCs include the lowered porosity, the evenly spaced distribution of reinforcements, the degree of solidification, and the density of reinforcements. Generally, the reinforcement materials are fragile and harder than the matrix material. By preventing dislocations from moving and preventing deformation, the abovementioned particles serve as strengthening agents when they are integrated into the matrix. Consequently, as compared to the matrix material alone, the hybrid AMCs show improved hardness.

3.5 Impact energy

The impact energy (IE) absorbed until the fracture by the squeeze-casted hybrid AMCs has been evaluated in this section. Figure 17 presented the impact energy results for various hybrid AMCs produced through squeeze casting, delineated by wt.% of reinforcement particles: (A) AA2024, (B) AA2024/Al_2O_3/SiC, (C) AA2024/Al_2O_3/SiC/Si_3N_4, (D) AA2024/Al_2O_3/SiC/BN, and (E) AA2024/Al_2O_3/SiC/Si_3N_4/BN. The outcomes highlight a clear relationship between the IE of hybrid AMCs and the increasing wt.% of reinforcements. Squeeze-casted AA2024, devoid of any reinforcements in the melt, exhibits the maximum impact energy (6.62 J). The results of the Charpy impact test demonstrated that the AA2024 specimen absorbed more energy, indicating that it would fracture more ductilely under room temperature plastic deformation. The ability of ductile materials to experience significant plastic deformation before breaking enables them to efficiently absorb impact energy. When it comes to AA2024, its ability to both absorb and deform energy during an impact event implies that impact energy can be absorbed and dispersed more efficiently, which increases impact resistance. So, Fig. 18's SEM analysis underscores a significant presence of dimple fractures and the propagation of cracks in the fractured samples of squeeze-casted AA2024, accompanied by the observation of dimple fracture.

Upon incorporating 2% Al_2O_3 and 2% SiC into the melt of AA2024, as illustrated in Fig. 17, the impact energy of the squeeze-casted AMC (AA2024/2%Al_2O_3/2%SiC) demonstrated a noteworthy decrease of 5.78 J, representing a 12.68% reduction over the base matrix material (AA2024). This energy reduction in the hybrid AMC is attributed to the wt.% of Al_2O_3 and SiC than the pristine AA2024 matrix. The impact strength of the developed hybrid AMC showed a reduction in strength and displayed brittle fracture characteristics, with stress concentration positions attributed to the introduction of brittle reinforcements. The presence of an Al_2O_3 clustering region around SiC particles was identified as a factor contributing to stress concentration, leading to increased stress in adjacent areas and initiating cracks. This phenomenon resulted in reduced toughness observed during the impact test. Despite this reinforcement, SEM analysis in Fig. 19 underscores the presence of porosity, cracks, and their propagation. The SEM analysis also reveals separated grain boundaries of α-Al and the presence of a particle crack, tear edges, and interfacial debonding on the fractured surface of the hybrid AMC (AA2024/2%Al_2O_3/2%SiC). The fractured sample exhibits a morphology characterized by a transgranular cleavage fracture.

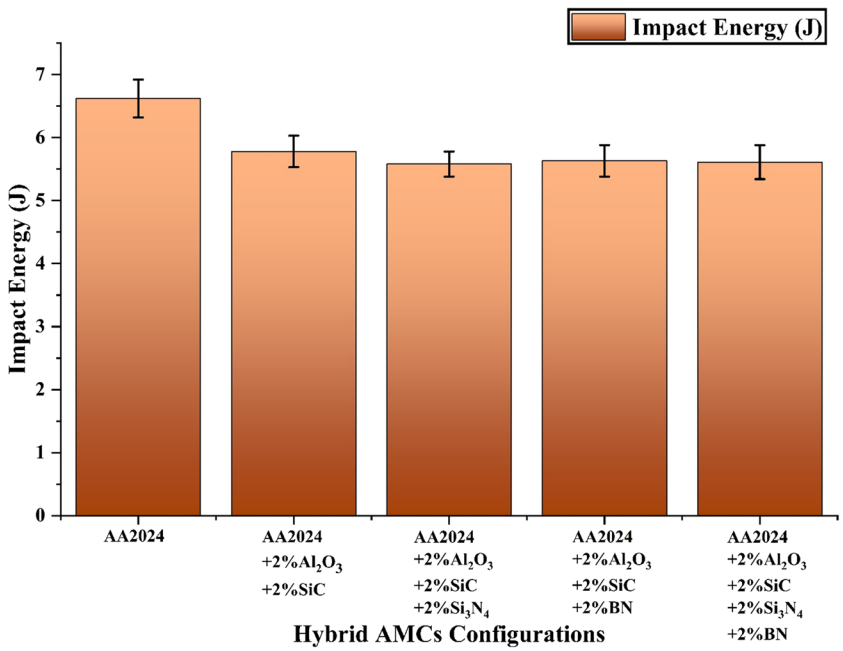

Fig. 17 Impact energy (J) analysis of hybrid AMC configurations

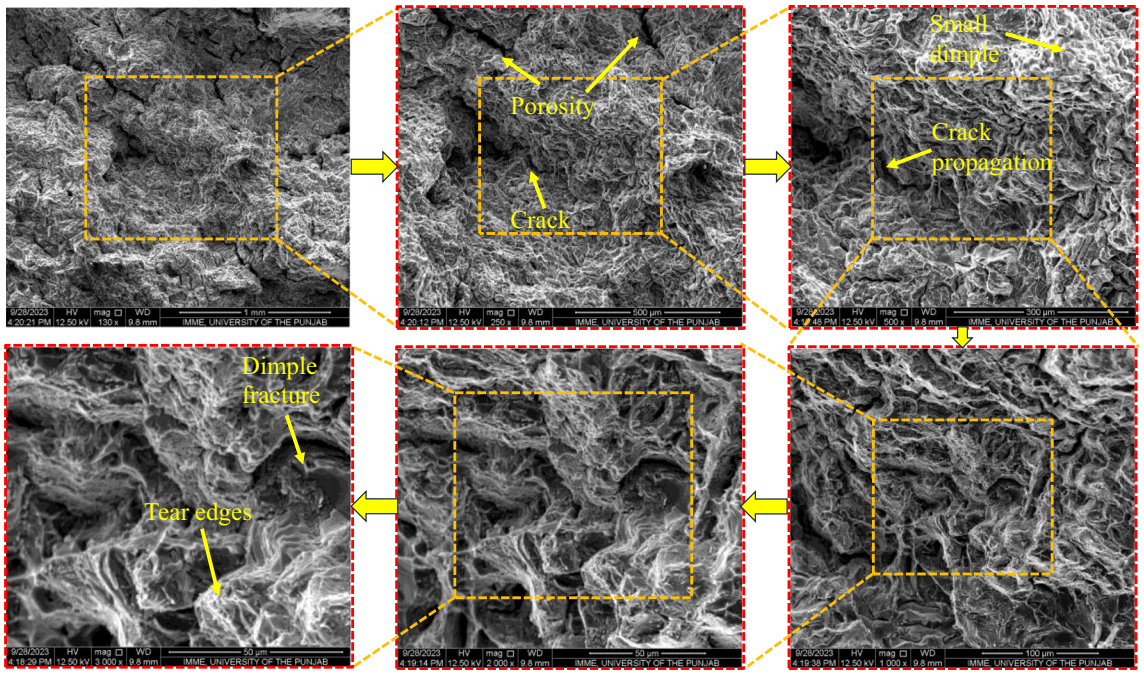

Fig. 18 SEM analysis of the fractured surface of squeeze-casted AA2024 Charpy impact specimen

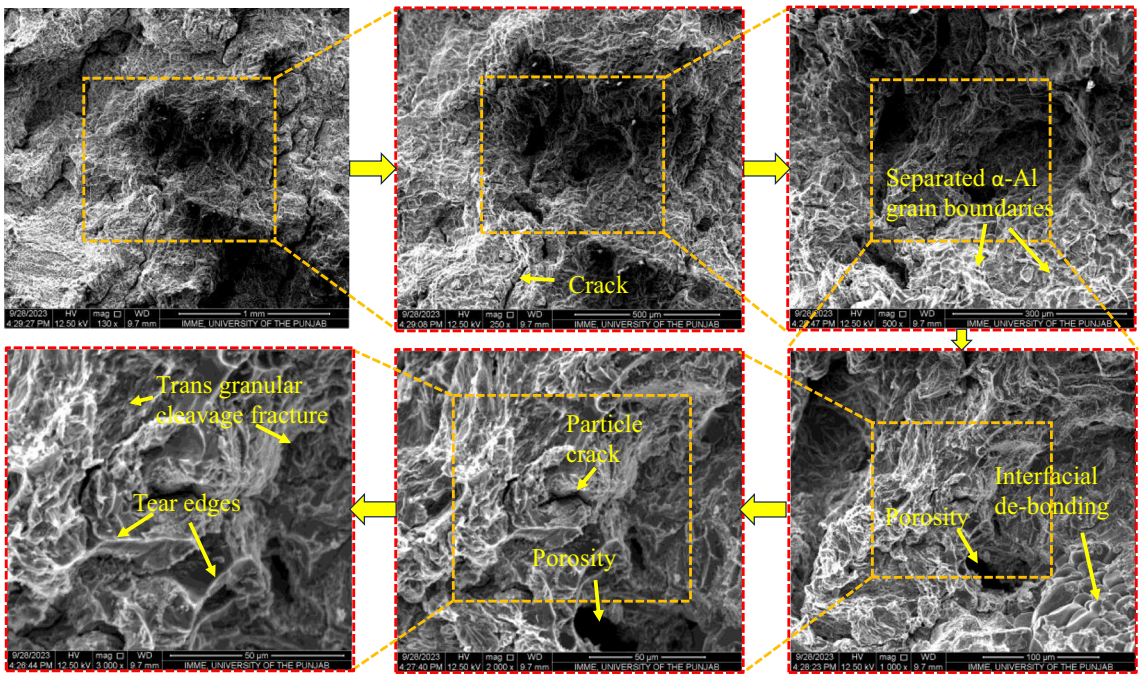

Fig. 19 SEM analysis of the fractured surface of squeeze-casted AA2024/2%Al_2O_3/2%SiC hybrid composite Charpy impact specimen

Analyzing the hybrid AMC containing 2% Al_2O_3, 2% SiC, and 2% Si_3N_4 in Fig. 17, it becomes apparent that this composition yields a lower impact strength of 5.58 J compared to AA2024 (6.62 J) and AA2024/2%Al_2O_3/2%SiC (5.78 J). The introduction of 2%Al_2O_3/2%SiC/2%Si_3N_4 reinforcement particles reduces the ductility of the hybrid AMC, reducing its impact energy. The impact energy of the hybrid AMC demonstrated a decrease in strength, manifesting brittle fracture characteristics characterized by stress concentration locations attributed to the incorporation of

reinforcements. The presence of AA2024 particles clustering around reinforcement particles (SiC and Si_3N_4) was identified as a factor contributing to stress concentration, resulting in increased stress in adjacent areas and the initiation of cracks. Moreover, the creation of clusters diminishes the interfacial bonding among the AA2024 and reinforcements, leading to a reduction in impact strength. This phenomenon contributed to the observed reduction in toughness during the impact test. SEM analysis of the fractured sample in Fig. 20 highlighted the transgranular cleavage fracture and intergranular fracture of the hybrid AMC (AA2024/2%Al_2O_3/2%SiC/2%Si_3N_4). Moreover, porosity, cracks, and their propagation are observed on the fractured surface of the hybrid AMC, where separated grain boundaries of α-Al have been identified.

The hybrid composite, denoted as AA2024/2%Al_2O_3/2%SiC/2%BN, exhibited a notably higher impact energy of 5.63 J. This IE value represents a substantial reduction of 14.95% compared to AA2024, a 2.59% reduction compared to AA2024/2%Al_2O_3/2%SiC, and a 0.89% increment compared to AA2024/2%Al_2O_3/2%SiC/2%Si_3N_4. The introduction of additional BN reinforcements comparatively reduces the hardness of hybrid AMC compared to the Si_3N_4 reinforcement particle and increasing the impact energy, as observed in Fig. 17. The incorporation of BN enhances the brittle nature and hence increased the impact energy of the developed hybrid AMC. The SEM analysis presented in Fig. 21 illustrates the interfacial debonding of the fractured specimen of the hybrid AMC (AA2024/2%Al_2O_3/2%SiC/2%BN), showcasing separated grain boundaries of α-Al. However, the analysis also reveals the presence of porosity, crack propagation, and transgranular cleavage fractures on the fractured surface of the hybrid AMC (AA2024/2%Al_2O_3/2%SiC/2%BN).

In general, the impact energy of hybrid AMC (AA2024/2%Al_2O_3/2%SiC/2%Si_3N_4/2%BN) tends to decrease (5.61 J) with a higher concentration of reinforcement particles (wt.% 8) within the AA2024, as depicted in Fig. 17. The primary reasons for this phenomenon are the effective transference of stress from the matrix to the reinforcements, distinctions in failure aspect between the reinforcement particles and alloy matrix, the induction of a high dislocation density in the matrix, and a decrease in composite grain size. Moreover, the impact energy of the hybrid AMC (AA2024/2%Al_2O_3/2%SiC/2%Si_3N_4/2%BN) exhibits a significant reduction: 15.26% compared to AA2024, 2.94% compared to AA2024/2%Al_2O_3/2%SiC, 0.54% increment compared to AA2024/2%Al_2O_3/2%SiC/2%Si_3N_4, and 0.89% reduction compared to AA2024/2%Al_2O_3/2%SiC/2%BN. The mechanical behavior seen in the fractography investigation indicates that there is enough internal flexibility in the AA2024 matrix alloy to allow for the redistribution of localized internal stresses, while the existence of 2%Al_2O_3/2%SiC/2%Si_3N_4/2%BN particles limits the plastic flow of the hybrid AMC, leading to fracture at lower impact energy. SEM analysis in Fig. 22 revealed interfacial debonding of the fractured specimen of the hybrid AMC

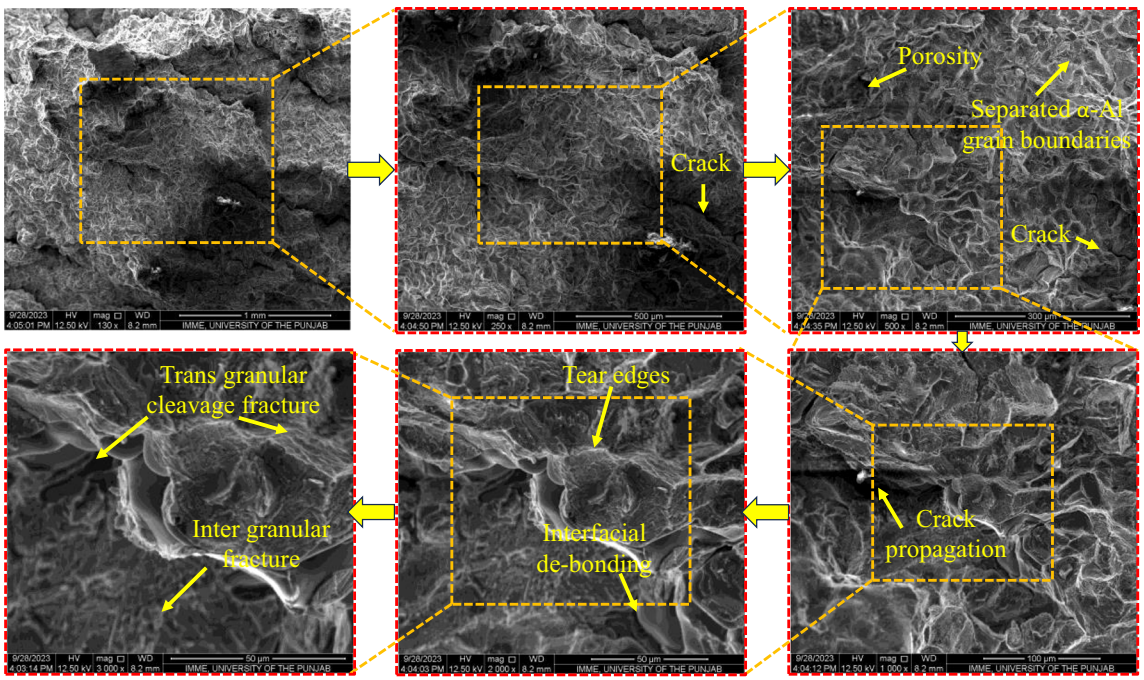

Fig. 20 SEM analysis of the fractured surface of squeeze-casted AA2024/2%Al_2O_3/2%SiC/2%Si_3N_4 hybrid composite Charpy impact specimen

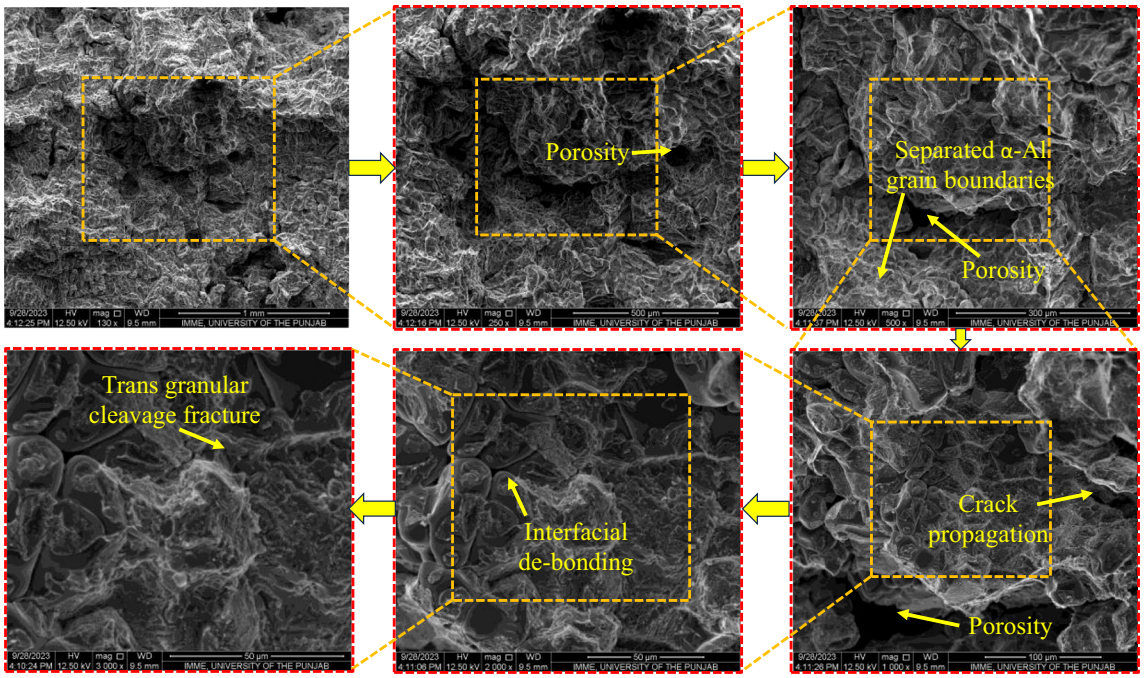

Fig. 21 SEM analysis of the fractured surface of squeeze-casted AA2024/2%Al_2O_3/2%SiC/2%BN hybrid composite Charpy impact specimen

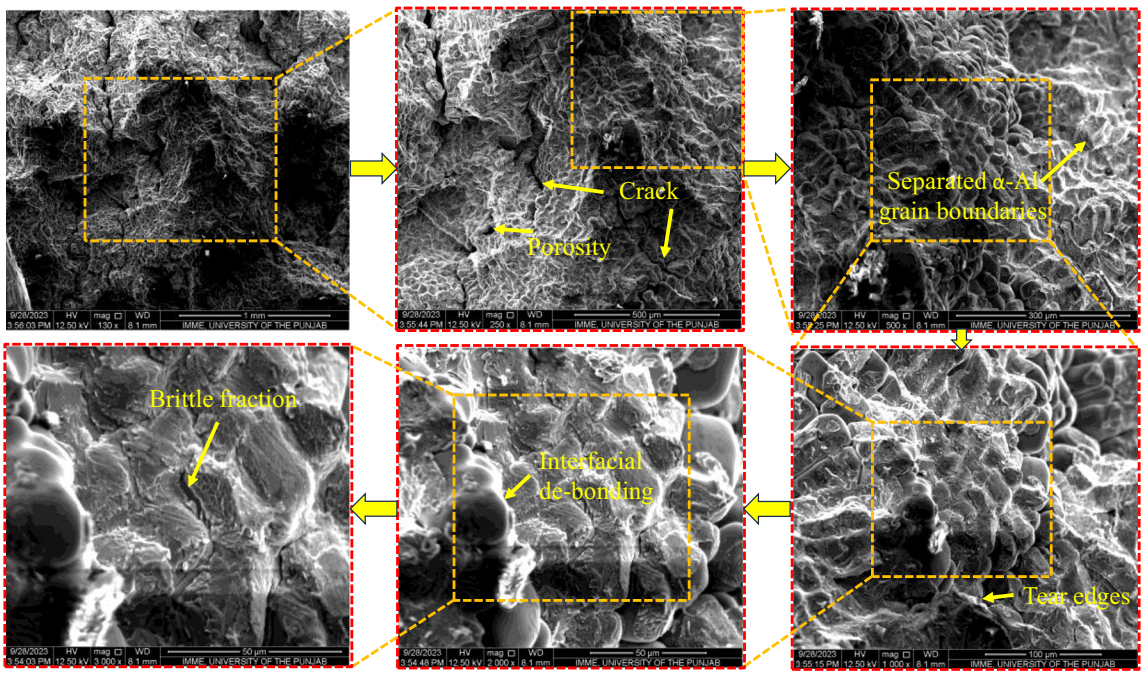

Fig. 22 SEM analysis of the fractured surface of squeeze-casted AA2024/2%Al_2O_3/2%SiC/2%Si_3N_4/2%BN hybrid composite Charpy impact specimen

(AA2024/2%Al_2O_3/2%SiC/2%Si_3N_4/2%BN), showcasing separated grain boundaries of α-Al. Additionally, porosity, crack propagation, and transgranular cleavage fractures are observed in the fractured SEM analysis of the hybrid AMC.

Generally, clusters inside the hybrid AMCs may emerge as a result of the inclusion of reinforced particulates (Al_2O_3, SiC, Si_3N_4, and BN). The material's overall homogeneity may be decreased, and stress concentrations may be created by these clusters, which would lower impact energy [65]. The interfacial bonding among the particles and the AA2024 may be broken by the increasing wt.% of reinforcement particles. In comparison to a more uniform matrix material like AA2024, this lower bonding weakens the structure overall and reduces impact resistance. A weaker interface may result from mismatches in the characteristics of the reinforcing particles and the matrix, such as differences in their coefficients of thermal expansion. The overall impact energy absorption capability is further reduced by the susceptibility of this weaker contact to failure under impact [51]. There may be an innate brittleness to several reinforcing particles, including Al_2O_3, SiC, Si_3N_4, and BN. This brittleness increases the composite's susceptibility to fracture upon impact by causing localized stress concentrations and crack initiation. The creation of flaws or areas of poor bonding might result from suboptimal processing conditions or an uneven distribution of particles, which can further reduce the impact energy absorption capacities.

3.6 Comparative analysis of the current study

In this section, a comparative analysis of the best configuration of AMC (AA2024/2%Al_2O_3/2%SiC/2%Si_3N_4/2%BN) with the squeeze-casted matrix material (AA2024) has been carried out for its mechanical characteristics (porosity %, UTS, EL%, hardness, and impact energy). It can be observed from Fig. 23 that squeeze-casted hybrid AMC AA2024/2%Al_2O_3/2%SiC/2%Si_3N_4/2%BN performed exceptionally well in giving the best values of response measures in comparison to the matrix material (AA2024). AA2024/2%Al_2O_3/2%SiC/2%Si_3N_4/2%BN outperformed in terms of UTS and hardness and gave 60.36% and 65.24%, respectively; however, the porosity, EL%, and impact energy have been compromised from the matrix material (AA2024) by 1.61%, 31.89%, and 15.26%, respectively. The reasons for the improvement and depreciation have been explained in the relevant sections above.

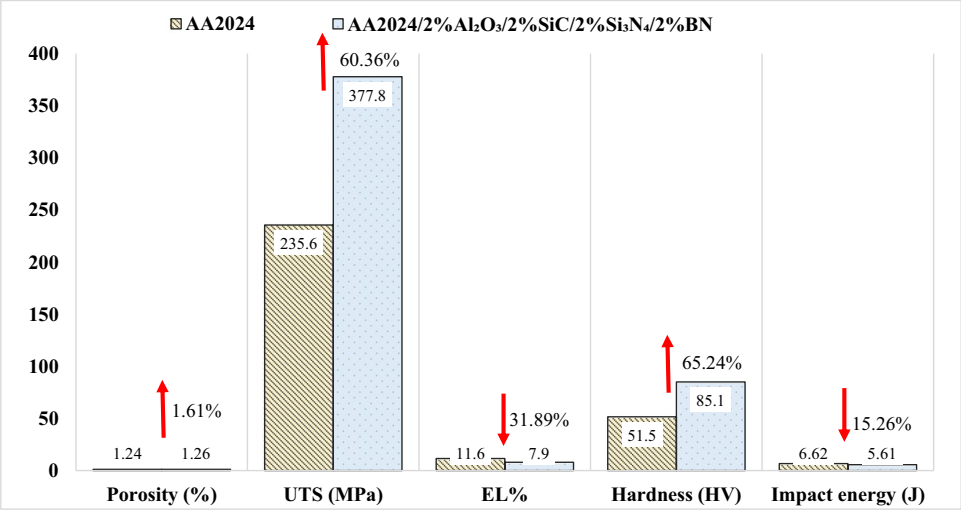

Fig. 23 Comparison of best configuration of hybrid AMC AA2024/2%Al2O3/2%SiC/2%Si3N4/2%BN with matrix material AA2024

Table 6 Comparison of current study's key findings with results from published studies on the AA2000 series

References	Materials	Hardness (HV)	Hardness (HRB)	UTS (MPa)	% Improvement of current study from published studies	
					Hardness	UTS
[28]	AA2026	125	69	281	18.92%	25.62%
[42]	AA2024-AA2024	121	68	280	20.10%	25.89%
[42]	AA2024-AA2024	128	70	297	17.74%	21.39%
[40]	AA2026-AA2026	130	71	315	16.57%	16.62%
[41]	AA2026/Al-4.5%Cu	140.76	75	326.91	11.87%	13.47%
Current study	AA2024/2%Al_2O_3/2%SiC/2%Si_3N_4/2%BN		85.1	377.8	-	-

Table 6 indicates the comparison of key findings of the best configuration of squeeze-casted hybrid AMC AA2024/2%Al_2O_3/2%SiC/2%Si_3N_4/2%BN current study with the published literature on the AA2000 series. It is illustrated in Table 6 that the results of hardness and UTS have been outperformed in comparison to other studies in the literature.

4 Conclusions

This investigation sought to fabricate hybrid AMCs utilizing varying wt.% of hybrid reinforcement particles, including Al_2O_3, SiC, Si_3N_4, and BN, employing stir-squeeze casting for AA2024. A comprehensive analysis of the impact of these hybrid reinforcement particles on the microstructural and mechanical characteristics of the AMCs was conducted, with a particular focus on porosity %, UTS (MPa), EL%, hardness (HRB), and impact energy (J). The microstructural assessment of the hybrid AMCs was carried out using both optical microscopy and SEM. Through this study, valuable insights have been gained into the intricate interplay between hybrid reinforcement particles and the resulting properties of AMCs, shedding light on the potential for enhanced performance in terms of strength, ductility, and impact resistance. After scrutinizing, the following conclusions are drawn from the above discussion:

1. It is evident from this research that with the addition of the wt.% of reinforcement particles (Al_2O_3, SiC, and Si_3N_4) to the matrix material up to 6%, the experimental density and porosity (%) of the hybrid AMCs have increased; however, a reverse trend has been observed when wt.% of BN of 2% is incorporated along with the abovementioned reinforcement particles. Maximum experimental density and porosity have been observed in squeeze-casted hybrid AMC AA2024/2%Al_2O_3/2%SiC/2%Si_3N_4 due to the higher densities of Al_2O_3, SiC, and Si_3N_4. However, AA2024/2%Al_2O_3/2%SiC/2%Si_3N_4/2%BN gave the best results in giving the lowest porosity (%) among the other hybrid configurations.
2. The effect of different wt.% of reinforcement particle on the UTS has also been explored, and it has been found that with the increasing wt.% of reinforcement particle in the matrix material (AA2024), the UTS has increased significantly. Among the fabricated hybrid AMCs, the AA2024/2%Al_2O_3/2%SiC/2%Si_3N_4/2%BN configuration gave the best results for UTS (377.8 MPa). Moreover, the UTS of the hybrid AMC with the composition AA2024/2%Al_2O_3/2%SiC/2%Si_3N_4/2%BN exhibits a noteworthy increase of 60.36% in comparison to pure AA2024, a 32.65% increment relative to AA2024/2%Al_2O_3/2%SiC, a 15.11% rise relative to AA2024/2%Al_2O_3/2%SiC/2%Si_3N_4, and an 11.87% improvement compared to AA2024/2%Al_2O_3/2%SiC/2%BN.
3. It has been found that the magnitude of EL% depreciates from 11.6 to 7.9 with the increment wt.% of reinforcement particles in AA2024. The observed EL% of 7.9% in the hybrid AMC with the composition AA2024/2%Al_2O_3/2%SiC/2%Si_3N_4/2%BN reveals a significant reduction of 31.89% compared to pure AA2024, an 18.56% decrease relative to AA2024/2%Al_2O_3/2%SiC, a 9.19% decrease when compared to AA2024/2%Al_2O_3/2%SiC/2%Si_3N_4, and a 4.82% decrease relative to AA2024/2%Al_2O_3/2%SiC/2%BN. This observed phenomenon can be attributed to the effective transfer of stress from the AA2024 to the reinforcements, facilitated by the induction of a high dislocation density in the hybrid AMC and the establishment of strong interfacial bonding.
4. The incorporation of hard reinforcement particles (Al_2O_3, SiC, Si_3N_4, and BN) into AA2024 results in a notable enhancement in hardness, transitioning from 51.5 to 85.1 HRB and transforming the material from a ductile to a brittle state. Specifically, the hardness of the hybrid AMC with the composition AA2024/2%Al_2O_3/2%SiC/2%Si_3N_4/2%BN demonstrates a substantial 65.24% increase compared to pure AA2024, a 29.53% increment relative to AA2024/2%Al_2O_3/2%SiC, a 14.08% rise compared to AA2024/2%Al_2O_3/2%SiC/2%Si_3N_4, and a 16.74% increase relative to AA2024/2%Al_2O_3/2%SiC/2%BN.
5. The investigation revealed a consistent decrease in impact energy magnitude, diminishing from 6.62 to 5.61 J as the wt.% of reinforcement particles increased in AA2024. Notably, the hybrid AMC, designated as AA2024/2%Al_2O_3/2%SiC/2%Si_3N_4/2%BN, exhibited a significantly elevated impact strength of 5.63 J. This strength value signifies a noteworthy reduction of 14.95% compared to AA2024, a 2.59% decrease relative to AA2024/2%Al_2O_3/2%SiC, and a marginal 0.89% increment compared to AA2024/2%Al_2O_3/2%SiC/2%Si_3N_4.
6. Fractography analysis of UTS and Charpy impact fractured samples depicts that a dimple fracture has been observed for the AA2024 without any reinforcement. However, with the addition of reinforcement particles (Al_2O_3, SiC), the fabricated AMC AA2024/2%Al_2O_3/2%SiC provided the cleavage fracture, while transgranular cleavage fractures have been observed in the fractured surfaces of the third and fourth configurations (AA2024/2%Al_2O_3/2%SiC/2%Si_3N_4, AA2024/2%Al_2O_3/2%SiC/2%BN). Moreover, the brittle fracture has been depicted in the broken sample of AA2024/2%Al_2O_3/2%SiC/2%Si_3N_4/2%BN.

Acknowledgements The authors are grateful to the Department of Industrial and Manufacturing Engineering, Faculty of

Mechanical Engineering, University of Engineering and Technology Lahore, Pakistan, for their assistance (ASRP Approved Funds No. ORIC/112-ASRB/2077).

Author contribution Conceptualization and methodology by Muhammad Asad Ali and Nadeem Ahmad Mufti; data curation, investigation, formal analysis, writing—original draft, validation, visualization, and review and editing by Muhammad Asad Ali; formal analysis, review and editing, resources, and supervision by Nadeem Ahmad Mufti; formal analysis and review and editing by Kashif Ishfaq; review and editing by Rakhshanda Naveed, Muhammad Qaiser Saleem, and Asif Mahmood Qureshi.

Declarations

Competing interests The authors declare no competing interests.

References

1. Bhoi NK, Singh H, Pratap S (2020) Developments in the aluminum metal matrix composites reinforced by micro/nano particles – a review. J Compos Mater 54:813–833. https://doi.org/10.1177/0021998319865307
2. Safri SNA, Sultan MTH, Jawaid M, Jayakrishna K (2018) Impact behaviour of hybrid composites for structural applications: a review. Compos B Eng 133:112–121. https://doi.org/10.1016/j.compositesb.2017.09.008
3. Zhou MY, Ren LB, Fan LL et al (2020) Progress in research on hybrid metal matrix composites. J Alloy Compd 838:155274. https://doi.org/10.1016/j.jallcom.2020.155274
4. Rahman Hafeezur A, Sundeep D, Sastry CC et al (2024) Investigation of ballistic and mechanical properties of AlNPB metal matrix composites reinforced with TiCN decorated graphene nano flakes for light armored vehicles. J Alloy Compd 992:174482. https://doi.org/10.1016/j.jallcom.2024.174482
5. Suthar J, Patel KM (2018) Processing issues, machining, and applications of aluminum metal matrix composites. Mater Manuf Processes 33:499–527. https://doi.org/10.1080/10426914.2017.1401713
6. Sharma SK, Saxena KK, Salem KH et al (2024) Effects of various fabrication techniques on the mechanical characteristics of metal matrix composites: a review. Adv Mater Process Technol 10:277–294. https://doi.org/10.1080/2374068X.2022.2144276
7. Kumar A, Singh VP, Singh RC et al (2024) A review of aluminum metal matrix composites: fabrication route, reinforcements, microstructural, mechanical, and corrosion properties. J Mater Sci 59:2644–2711. https://doi.org/10.1007/s10853-024-09398-7
8. Samal P, Vundavilli PR, Meher A, Mahapatra MM (2020) Recent progress in aluminum metal matrix composites: a review on processing, mechanical and wear properties. J Manuf Process 59:131–152. https://doi.org/10.1016/j.jmapro.2020.09.010
9. Arulraj M, Palani PK (2018) Parametric optimization for improving impact strength of squeeze cast of hybrid metal matrix (LM24–SiCp–coconut shell ash) composite. J Braz Soc Mech Sci Eng 40:2. https://doi.org/10.1007/s40430-017-0925-3
10. Sadagopan P, Natarajan HK, Praveen Kumar J (2018) Study of silicon carbide-reinforced aluminum matrix composite brake rotor for motorcycle application. Int J Adv Manuf Technol 94:1461–1475. https://doi.org/10.1007/s00170-017-0969-7
11. Wang ZJ, Zheng Z, Fu MW (2024) Aluminum matrix composites: structural design and microstructure evolution in the deformation process. J Market Res 30:3724–3754. https://doi.org/10.1016/j.jmrt.2024.03.237
12. Garg P, Jamwal A, Kumar D et al (2019) Advance research progresses in aluminium matrix composites: manufacturing & applications. J Market Res 8:4924–4939. https://doi.org/10.1016/j.jmrt.2019.06.028
13. Gupta S, Giri A, Adhikari S, Srivastava V (2018) Development and characterization of in-situ aluminum–titanium carbide composites prepared by pneumatic powder injection route. In: Srivatsan TS, Zhang Y, Harrigan WC (eds) Metal-matrix composites innovations, advances and applications. Springer International Publishing, Cham, pp 59–68
14. Siva R, Vimalson KA, Yogeshkumar P et al (2021) Study on optimization of spur gear performance with titanium carbide incorporated aluminium matrix composite. Mater Today Proc 44:3686–3691. https://doi.org/10.1016/j.matpr.2020.10.804
15. Su WX, Wang HM, Li GR, Zhang YF (2024) Evolution of microstructure and mechanical properties of aluminum matrix composites reinforced with dual-phase heterostructures. Mater Sci Eng A 901:146500. https://doi.org/10.1016/j.msea.2024.146500
16. Upadhyay G, Saxena KK (2021) Role of stir casting in development of aluminium metal matrix composite (AMC): an overview. IOP Conf Ser Mater Sci Eng 1116:012022. https://doi.org/10.1088/1757-899X/1116/1/012022
17. Deng J, Xie B, You D, Huang H (2023) Review of design of process parameters for squeeze casting. Chin J Mech Eng 36:146. https://doi.org/10.1186/s10033-023-00979-2
18. Sp VG, Sk S (2023) Effect of ultrasonic treatment during stir casting on mechanical properties of AA6063-SiC composites. Mater Chem Phys 294:126977. https://doi.org/10.1016/j.matchemphys.2022.126977
19. Sankhla A, Patel KM (2022) Metal matrix composites fabricated by stir casting process–a review. Adv Mater Process Technol 8:1270–1291. https://doi.org/10.1080/2374068X.2020.1855404
20. Sheikh KA, Mir FA (2024) Microstructural evolution and wear dynamics of Al5052/cenosphere metal matrix composite fabricated through compo-casting technique. Trans Indian Inst Met. https://doi.org/10.1007/s12666-024-03370-4
21. Aneesh T, Pawan K, Mohan L et al (2022) Exploring casting defects of AA7075 alloy in the gravity die casting simulation of an IC engine block. Proc Inst Mech Eng Part E J Process Mech Eng 236:1556–1565. https://doi.org/10.1177/09544089211073296
22. Mohapatra S, Sarangi H, Mohanty UK (2020) Effect of processing factors on the characteristics of centrifugal casting. Manuf Rev 7:26. https://doi.org/10.1051/mfreview/2020024
23. Mishra SS, Chaira D (2022) Fabrication and characterisation of (Si3N4-Mo)-Al/Si cermet by pressure-less melt infiltration. Mater Today Proc 51:2321–2326. https://doi.org/10.1016/j.matpr.2021.11.533
24. Ghasali E, Alizadeh M, Ebadzadeh T (2016) Mechanical and microstructure comparison between microwave and spark plasma sintering of Al–B4C composite. J Alloy Compd 655:93–98. https://doi.org/10.1016/j.jallcom.2015.09.024
25. Ibrahim MA, Sahin Y, Gidado AY, Said M (2019) Mechanical properties of aluminium matrix composite including SiC/Al2O3 by powder metallurgy-a review. GSJ 7:23–38
26. Sama SR, Badamo T, Lynch P, Manogharan G (2019) Novel sprue designs in metal casting via 3D sand-printing. Addit Manuf 25:563–578. https://doi.org/10.1016/j.addma.2018.12.009
27. Serrano-Munoz I, Buffiere J-Y, Verdu C (2018) Casting defects in structural components: are they all dangerous? A 3D study. Int J Fatigue 117:471–484. https://doi.org/10.1016/j.ijfatigue.2018.08.019
28. Ali MA, Ishfaq K, Jawad M (2019) Evaluation of surface quality and mechanical properties of squeeze casted AA2026 aluminum alloy using response surface methodology. Int J Adv Manuf Technol 103:4041–4054. https://doi.org/10.1007/s00170-019-03836-6

29. Adesoji Adediran A, Babafemi Ogunkola A, Odikpo Edoziuno F et al (2022) Squeeze casting process: trends and opportunities. In: R. Vijayaram T (ed) Casting processes. IntechOpen. https://doi.org/10.5772/intechopen.103764
30. Singh J, Jawalkar CS, Belokar RM (2020) Analysis of mechanical properties of AMC fabricated by vacuum stir casting process. Silicon 12:2433–2443. https://doi.org/10.1007/s12633-019-00338-8
31. Mourad A-HI, Christy JV, Krishnan PK, Mozumder MS (2023) Production of novel recycled hybrid metal matrix composites using optimized stir squeeze casting technique. J Manuf Process 88:45–58. https://doi.org/10.1016/j.jmapro.2023.01.040
32. Christy JV, Arunachalam R, Mourad A-HI et al (2020) Processing, properties, and microstructure of recycled aluminum alloy composites produced through an optimized stir and squeeze casting processes. J Manuf Process 59:287–301. https://doi.org/10.1016/j.jmapro.2020.09.067
33. Muraliraja R, Arunachalam R, Al-Fori I, Al-Maharbi M, Piya S (2019) Development of alumina reinforced aluminum metal matrix composite with enhanced compressive strength through squeeze casting process. Proc Inst Mech Eng Part L J Mater Des Appl 233(3):307–314. https://doi.org/10.1177/1464420718809516
34. Kumar MS, Mangalaraja RV, Kumar RS, Natrayan L (2019) Processing and characterization of AA2024/Al2O3/SiC reinforces hybrid composites using squeeze casting technique. Iran J Mater Sci Eng 16(2):55–67
35. Lu T, Chen W, Li B et al (2019) Influence mechanisms of Zr and Fe particle additions on the microstructure and mechanical behavior of squeeze-cast 7075Al hybrid composites. J Alloy Compd 798:587–596. https://doi.org/10.1016/j.jallcom.2019.05.301
36. Gecu R, Karaaslan A (2019) A comparative study on titanium-reinforced aluminium matrix composites produced by melt infiltration casting and squeeze infiltration. Inter Metalcast 13:311–319. https://doi.org/10.1007/s40962-018-0253-0
37. Natrayan L, Senthil Kumar M, Chaudhari M (2020) Optimization of squeeze casting process parameters to investigate the mechanical properties of AA6061/Al2O3/SiC hybrid metal matrix composites by Taguchi and ANOVA approach. In: Venkata Rao R, Taler J (eds) Advanced Engineering Optimization Through Intelligent Techniques. Springer Singapore, Singapore, pp 393–406
38. Idrisi AH, Mourad A-HI (2019) Conventional stir casting versus ultrasonic assisted stir casting process: mechanical and physical characteristics of AMCs. J Alloy Compd 805:502–508. https://doi.org/10.1016/j.jallcom.2019.07.076
39. Chak V, Chattopadhyay H (2023) Mechanical and tribological properties of ceramic–aluminium composites developed using stirring-assisted squeeze casting. Int J Cast Met Res 36:65–75. https://doi.org/10.1080/13640461.2023.2207894
40. Ali MA, Ishfaq K, Raza MH et al (2020) Mechanical characterization of aged AA2026-AA2026 overcast joints fabricated by squeeze casting. Int J Adv Manuf Technol 107:3277–3297. https://doi.org/10.1007/s00170-020-05242-9
41. Ahmed N, Ali MA, Raza MH et al (2024) Squeeze overcasting of bimetallic composite Al2026/Al–4.5%Cu with acidic quenching in aging treatment: characterization of mechanical properties and joint interface microstructure. Inter Metalcast 18:1644–1663. https://doi.org/10.1007/s40962-023-01141-3
42. Ali MA, Jahanzaib M, Wasim A et al (2018) Evaluating the effects of as-casted and aged overcasting of Al-Al joints. Int J Adv Manuf Technol 96:1377–1392. https://doi.org/10.1007/s00170-018-1682-x
43. Raza MH, Ali MA, Tahir W et al (2021) Cryogenic treatment analysis of electrodes in wire electric discharge machining of squeeze casted Al2024/Al2O3/W composite. Int J Adv Manuf Technol 116:1179–1198. https://doi.org/10.1007/s00170-021-07521-5
44. Zhou X, Gao Y, Wang Y et al (2022) The aging behavior of Ni-coated carbon fibers and ZrC particles reinforced 2024Al matrix composites. J Alloy Compd 917:165468. https://doi.org/10.1016/j.jallcom.2022.165468
45. Ahmed N, Raza MH, Ali MA et al (2024) Analyzing the dimensional errors in wire electric discharge machining of squeeze casted Al2024/Al2O3/W composite using cryogenic treated electrodes. J Market Res 29:476–490. https://doi.org/10.1016/j.jmrt.2024.01.125
46. Shalaby EAM, Churyumov AYu, Solonin AN, Lotfy A (2016) Preparation and characterization of hybrid A359/(SiC+Si3N4) composites synthesized by stir/squeeze casting techniques. Mater Sci Eng A 674:18–24. https://doi.org/10.1016/j.msea.2016.07.058
47. Sajjadi SA, Ezatpour HR, Torabi Parizi M (2012) Comparison of microstructure and mechanical properties of A356 aluminum alloy/Al2O3 composites fabricated by stir and compo-casting processes. Mater Des 34:106–111. https://doi.org/10.1016/j.matdes.2011.07.037
48. Amouri K, Kazemi Sh, Momeni A, Kazazi M (2016) Microstructure and mechanical properties of Al-nano/micro SiC composites produced by stir casting technique. Mater Sci Eng A 674:569–578. https://doi.org/10.1016/j.msea.2016.08.027
49. Raza MH, Wasim A, Ali MA et al (2018) Investigating the effects of different electrodes on Al6061-SiC-7.5 wt% during electric discharge machining. Int J Adv Manuf Technol 99:3017–3034
50. Ramadoss N, Pazhanivel K, Anbuchezhiyan G (2020) Synthesis of B4C and BN reinforced Al7075 hybrid composites using stir casting method. J Market Res 9:6297–6304
51. Chandla NK, Yashpal KS et al (2020) Experimental analysis and mechanical characterization of Al 6061/alumina/bagasse ash hybrid reinforced metal matrix composite using vacuum-assisted stir casting method. J Compos Mater 54:4283–4297. https://doi.org/10.1177/0021998320929417
52 Zyska A, Boroń K (2021) Comparison of the porosity of aluminum alloys castings produced by squeeze casting. Manuf Technol 21:725–734. https://doi.org/10.21062/mft.2021.074
53. Mufti NA, Islam MU, Ali MA et al (2022) Analysis of annealing on the micro-porosity and ductility of squeeze-casted Al7050 alloy for the structural applications. ArchivCivMechEng 22:107. https://doi.org/10.1007/s43452-022-00428-2
54. Ramadoss N, Pazhanivel K, Ganeshkumar A, Arivanandhan M (2023) Microstructural, mechanical and corrosion behaviour of B4C/BN-reinforced Al7075 matrix hybrid composites. Inter Metalcast 17:499–514. https://doi.org/10.1007/s40962-022-00791-z
55. Thamilarasan J, Karthik K, Balaguru S et al (2023) An investigation on the mechanical properties of graphene nanocomposite. In: Sethuraman B, Jain P, Gupta M (eds) Recent advances in mechanical engineering. Springer Nature Singapore, Singapore, pp 483–492
56. Senthil Kumar M, Natrayan L, Hemanth RD et al (2018) Experimental investigations on mechanical and microstructural properties of Al $_2$ O $_3$ /SiC reinforced hybrid metal matrix composite. IOP Conf Ser Mater Sci Eng 402:012123. https://doi.org/10.1088/1757-899X/402/1/012123
57. Umanath K, Palanikumar K, Selvamani ST (2013) Analysis of dry sliding wear behaviour of Al6061/SiC/Al2O3 hybrid metal matrix composites. Compos B Eng 53:159–168. https://doi.org/10.1016/j.compositesb.2013.04.051
58. Farajollahi R, Jamshidi Aval H, Jamaati R (2022) Evaluating of the microstructure, texture, and mechanical properties of AA2024-Al3NiCu composites fabricated by the stir casting process. CIRP J Manuf Sci Technol 37:204–218. https://doi.org/10.1016/j.cirpj.2022.01.013
59. Singh B, Kumar I, Saxena KK et al (2023) A future prospects and current scenario of aluminium metal matrix composites

characteristics. Alex Eng J 76:1–17. https://doi.org/10.1016/j.aej.2023.06.028
60. Bhaskar S, Kumar M, Patnaik A (2022) Effect of Si3N4 ceramic particulates on mechanical, thermal, thermo-mechanical and sliding wear performance of AA2024 alloy composites. Silicon 14:239–262. https://doi.org/10.1007/s12633-020-00810-w
61. Lu Y, Yang J, Lu W et al (2010) The mechanical properties of co-continuous Si3N4/Al composites manufactured by squeeze casting. Mater Sci Eng A 527:6289–6299. https://doi.org/10.1016/j.msea.2010.06.047
62. Kumar A, Singh RC, Chaudhary R (2022) Investigation of nano-Al2O3 and micro-coconut shell ash (CSA) reinforced AA7075 hybrid metal–matrix composite using two-stage stir casting. Arab J Sci Eng 47:15559–15573. https://doi.org/10.1007/s13369-022-06728-2
63. Du WB, Tatsuzawa K, Aizawa T, Kihara J (2001) Processing and characterization of alumina wire by controlled fracture forming process::(I) Forming behavior and evolution of green microstructure. Mater Sci Eng A 316(1–2):238–247. https://doi.org/10.1016/S0921-5093(01)01241-2
64. Krishna SA, Noble N, Radhika N, Saleh B (2024) A comprehensive review on advances in high entropy alloys: Fabrication and surface modification methods, properties, applications, and future prospects. J Manuf Process 109:583–606. https://doi.org/10.1016/j.jmapro.2023.12.039
65. Pandian V, Kannan S (2021) Processing and preparation of aerospace-grade aluminium hybrid metal matrix composite in a modified stir casting furnace integrated with mechanical supersonic vibration squeeze infiltration method. Mater Today Commun 26:101732. https://doi.org/10.1016/j.mtcomm.2020.101732

Publisher's Note Springer Nature remains neutral with regard to jurisdictional claims in published maps and institutional affiliations.

Springer Nature or its licensor (e.g. a society or other partner) holds exclusive rights to this article under a publishing agreement with the author(s) or other rightsholder(s); author self-archiving of the accepted manuscript version of this article is solely governed by the terms of such publishing agreement and applicable law.